scientific reports

Check for updates

OPEN

Pt-LIS1 participates nuclear deformation and acrosome formation via regulating Dynein-1 during spermatogenesis in *Portunus trituberculatus*

Le Chang, Qiu Meng Xiang, Zai-Tian Liao, Jun-Quan Zhu, Chang-Kao Mu, Chun-Lin Wang & Cong-Cong Hou✉

Spermatogenesis involves complex dynamic mechanisms. Dynein-1 is a key carrier in cellular cargo transport, participating in nuclear deformation and acrosome formation during spermatogenesis. However, the regulatory mechanisms of Dynein-1 during cargo transport remain unknown. In this study, we explored the role of Lissencephaly 1 (LIS1) in spermatogenesis and its impact on Dynein-1 cargo transport in *Portunus trituberculatus*. LIS1 was known as a Dynein-1 regulator, which is a causative gene of anencephaly syndrome. *Pt-Lis1* was cloned from the crab testis, and its highly expression was observed in the testis. Pt-LIS1 dynamically localized around the nucleus and acrosome during spermatogenesis, colocalizing with Dynein-1 subunits, microtubules, mitochondrial markers (PHB), and Acrosin. RNA interference reduced *Pt-Lis1* expression, leading to decreased expression of *Pt-dhc* and *Pt-dic*. During spermatogenesis, the signals of Pt-LIS1, Pt-DHC, Pt-DIC, and α-Tubulin were weakened and showed disorganized distribution. The colocalization of Pt-LIS1 with Pt-DHC and Pt-DIC decreased, while abnormal colocalization significantly increased. In addition, *caspase-3* and *p53* expression significantly increased after *Pt-Lis1* silencing, indicating association with apoptosis in spermatogenic cells. All these results suggest that LIS1 played a crucial role in crustacean spermatogenesis by regulating nuclear deformation and acrosome formation through modulating Dynein-1 transport cargoes along microtubules.

Keywords Crustacean, Motor protein, Intracellular transport, Regulation, RNA interference

Spermatogenesis is a highly complex physiological process that is coordinated in a well-regulated stepwise manner by various cell factors and signaling pathways and is involved in mitosis, meiosis and spermiogenesis[1,2]. In mammals, spermatids undergo cytoplasmic discarding, nuclear deformation, acrosome formation and tail formation, which eventually develop into mature sperm with athletic ability[3,4]. However, in crustaceans, mature sperm have a unique structure, showing irregular morphology, usually without a tail, and are nonmotile sperm without flagella[5,6]. During spermatogenesis, the spermatid nucleus undergoes compression and deformation, ultimately forming a highly condensed sperm nucleus. This process is a crucial step in sperm development, enabling the sperm to reduce in volume and adapt to its specialized function and environment. The sperm nucleus morphology of crustaceans also varies according to different groups. In the Brachyura suborder, the nucleus of mature sperm is cup-shaped and wrapped around the acrosomal periphery[7]. In the swimming suborder, most of the sperm nucleus of *Macrobrachium* are disc-shaped, while the sperm nucleus of *Penaeus* are spherical[8,9]. In Brachyura suborder, the sperm nucleus is cup-shaped and wrapped around the acrosome[10]. In early spermatids, the acrosome particles produced by rough endoplasmic reticulum were dispersed in the cytoplasm. In the middle stage of spermatids, they gradually aggregated to form large acrosomal vesicles localized on one side of the cell, and in late spermatids, they gradually specialized into an acrosomal structure consisting of an acrosomal cap, an acrosomal tube, an intermediate layer, a filamentous layer, and a lamellipodium, which

Key Laboratory of Applied Marine Biotechnology By the Ministry of Education and Key Laboratory of Marine Biotechnology of Zhejiang Province, School of Marine Sciences, Ningbo University, Ningbo 315832, China. ✉email: houcongcong@nbu.edu.cn

involves complex dynamic mechanisms. The mature sperm of *P. trituberculatus* have the typical structure of the Brachyura suborder.

Motor proteins are the main driving force of intracellular transportation and cell deformation and use the cytoskeleton as a motor track to transport cellular cargo to specific sites for physiological functions in a precise and efficient manner[11]. Cytoplasmic Dynein-1 (Dynein-1), a large molecular complex of motor proteins, consists of four types of subunits: heavy chain, intermediate chain, light chain and light intermediate chain[12,13]. Dynein-1 is mainly responsible for the transport of various cargoes in the cytoplasm, including membranous organelles (lysosomes, Golgi bodies, mitochondria, etc.), mRNA, viruses, protein complexes (such as mitotic checkpoint proteins), etc.[14]. Dynein-1 plays an important role in spermatogenesis in *Rattus norvegicus*. Disruption of dynein function by either RNA interference (RNAi) or Ciliobrevin D inhibitors affected the formation of the blood-testis barrier and disrupt spermatogenesis, leading to an increase in abnormal spermatids[15]. In *P. trituberculatus*, Dynein-1 is involved in nuclear deformation and acrosome formation in spermatogenesis[16,17]. At present, how Dynein-1 is regulated during cellular cargo transport in spermatogenesis remains unknown. However, studies have shown that in mammalian neuronal cells, Dynein-1 collaborates with its regulatory protein LIS1 to accomplish complex cellular activities[18].

LIS1, as one of the important regulators of Dynein-1, binds to Dynein-1 through its C-terminal structural domain and changes Dynein-1 from an autoinhibitory state (Phi conformation) to an activated state[19], thus participating in Dynein-1-mediated intracellular transport, nuclear migration, and localization of the spindle and organelles[20]. At present, researches on the function of LIS1 mainly focus on the mechanism of the migration, survival, and proliferation of vertebrate nerve cells[21–23]. A few studies have also shown that LIS1 is indispensable for sperm acrosome formation in mouse spermatogenesis and that *Lis1* deficiency results in blocked acrosome formation, irregular nuclear morphology, abnormal apoptosis of spermatogenic cells, and even embryo death[18,24]. In *Drosophila* spermatogenesis, LIS1 is closely associated with spermatid nucleus deformation, localization and acrosome formation by regulating Dynein-1-mediated centrosome localization[25]. To date, the role and specific mechanism of LIS1 in the spermatogenesis of *P. trituberculatus* remains unknown.

The purpose of our research is to investigate the role of Pt-LIS1 in the spermatogenesis of *P. trituberculatus* and identify how Pt-LIS1 is involved in the regulation of cargo transport by Dynein-1. In the present study, we firstly cloned the full-length cDNA of the *Pt-Lis1*. Then, we utilized qPCR, fluorescence in situ hybridization (FISH), immunofluorescence (IF), Hematoxylin and eosin staining (HE), Western blotting (WB), and RNAi to investigate the expression, distribution and function of Pt-LIS1 during spermatogenesis, including spermatogonial mitosis, spermatocyte meiosis, acrosome formation, nuclear shaping and the maintenance of testicular homeostasis.

Results

Identification and characterization of the *Pt-Lis1* gene in *P. trituberculatus*

The full length of *Pt-Lis1* (GenBank accession no. OL841528) cDNA is 1844 bp, with a 1230 bp open reading frame (ORF), a 146 bp 5′ untranslated region (UTR), and a 468 bp 3′UTR, encoding 410 amino acids (aa) (Fig. 1A). The molecular weight of Pt-LIS1 was 46 kDa, and the isoelectric point was 4.99. The similarities of the LIS1 protein sequence with its homologous sequences in *Homo sapiens* (GenBank accession no. NM_000430.4), *Mus musculus* (GenBank accession no. NM_013625.4), *Xenopus laevis* (GenBank accession no. NM_205830.1), *Larimichthys crocea* (GenBank accession no. NM_027273497.1), *Drosophila melanogaster* (GenBank accession no. NM_001259432.2), *Penaeus monodon* (GenBank accession no. NM_037922710.1), *Penaeus vannamei* (GenBank accession no. NM_027355967.1) and *Penaeus japonicus* (GenBank accession no. NM_043022649.1) were 84.2, 84.2, 84.0, 83.5, 86.4, 96.8, 96.8 and 97.1%, respectively (Fig. 1B).

We predicted the structural domain of Pt-LIS1 using the online tools SMART and CD-Search. Pt-LIS1 includes the LISH domain at the N-terminus (9–41 aa) and the β-propeller domain at the C-terminus, consisting of seven WD40 structural domains (97–136 aa, 139–178 aa, 181–220 aa, 223–262 aa, 265–324 aa, 327–366 aa, and 369–408 aa) (Fig. 1C). The phylogenetic analysis revealed that Pt-LIS1 clusters with homologs from crustaceans such as *Homarus americanus* and *P. japonicus*, showing a closer evolutionary relationship with insects, while exhibiting a more distant connection to vertebrates (Fig. 1D).

The highly expression and distribution of *Pt-Lis1* in the testis of *P. trituberculatus*

The semiquantitative PCR results revealed ubiquitous expression of *Pt-Lis1* mRNA across all tissues examined in *P. trituberculatus*. However, its expression was notably high in the testis (Fig. 2A, B). The distribution of *Pt-Lis1* mRNA in the testis of *P. trituberculatus* during spermiogenesis through FISH experiments. In early spermatids, *Pt-Lis1* mRNA exhibited uniform distribution in the cytoplasm around the nucleus (Fig. 2CA1-A3). In the middle stage of spermatids, *Pt-Lis1* mRNA was found in the cytoplasm on the opposite side of the nucleus (Fig. 2CB1-B3). In late spermatids, as the nucleus gradually compressed into a cup shape, *Pt-Lis1* mRNA predominantly localized on the inner side of the cup-shaped nucleus, with a small amount also present in the acrosomal tube (Fig. 2CC1-C3). The distribution of *Pt-Lis1* continuously changes with nuclear deformation, suggesting its potential involvement in this process. Finally, in mature sperm, *Pt-Lis1* mRNA was primarily concentrated in the acrosome tube and acrosome cap (Fig. 2CD1-D3). The negative control did not detect signals other than DAPI (Fig. 2CA5-D7), demonstrating the specificity of the *Pt-Lis1* mRNA probe. The localization pattern of the *Pt-Lis1* mRNA signal in different stages of spermiogenesis was plotted according to the localization results (Fig. 2CA4-D4).

Distribution of Pt-LIS1 protein in the testis of *P. trituberculatus*

To examine the expression pattern of Pt-LIS1 in the testis of *P. trituberculatus*, antibodies against Pt-LIS1 were developed. Initially, peptide fragments were expressed in Transetta (DE3) competent cells and then injected into

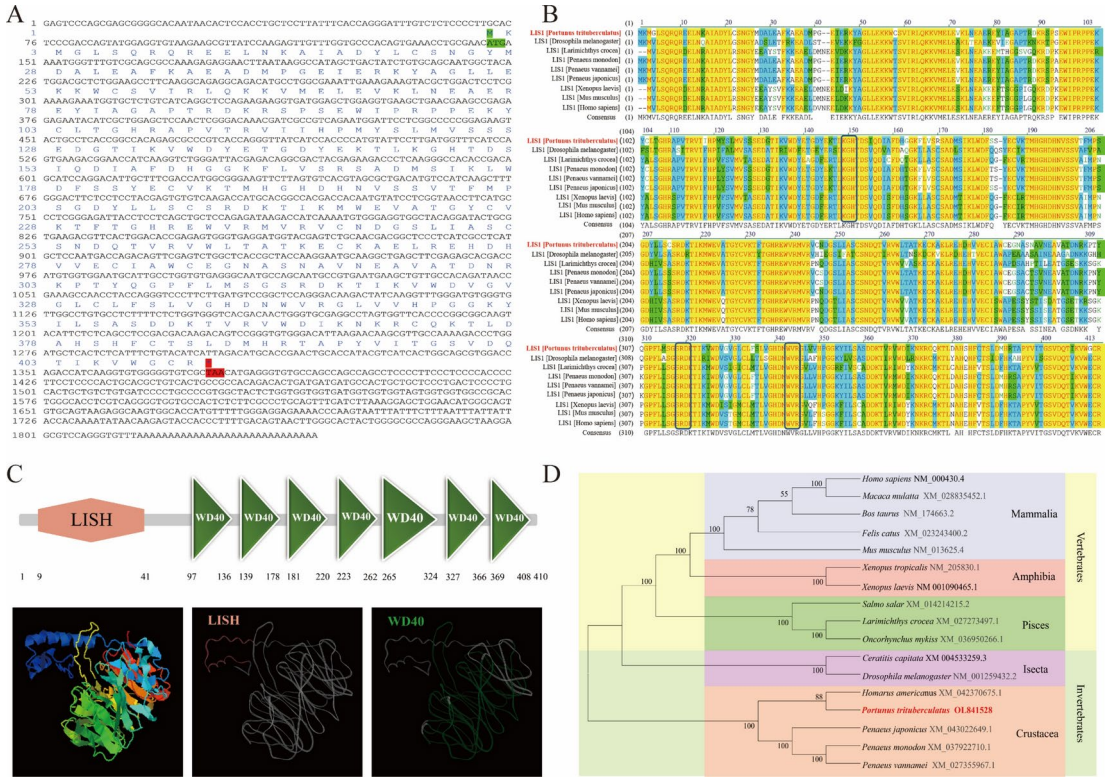

Fig. 1. Identification and characterization of the *Pt-Lis1* gene. (**A**) Full-length sequence of cDNA and corresponding amino acids of the *Pt-Lis1 gene*. The full length of *Pt-Lis1* cDNA is 1844 bp, encoding 410 amino acids (blue). The green marker is the start codon, and the red marker is the termination codon. (**B**) Amino acid multiple sequence alignment of LIS1. LIS1 in vertebrates and invertebrates is highly conserved in evolution. (**C**) Secondary structure and tertiary structure of the Pt-LIS1 protein. (c') Secondary structure of the Pt-LIS1 protein. The pink region is the LISH domain (aa: 9–41), the green region is seven consecutive WD40 domains (aa: 97–136, 139–178, 181–220, 223–262, 265–324, 327–366, 369–408); (c''-c'''') Tertiary structure of the Pt-LIS1 protein; (c''') Tertiary structure of the LISH domain; (c'''') Tertiary structure of the WD40 domain. (**D**) Phylogenetic tree of LIS1. *P. trituberculatus* is marked by red bold font. LIS1 had the closest relationship with *H. americanus* and clustered with other Decapoda animals in the same branch. It is closely related to insects and far from vertebrates.

SD rats and New Zealand rabbits. Antibodies were subsequently obtained from the serum of rats and rabbits, revealing specific bands corresponding to Pt-LIS1 at 46 kDa (Fig. 3A-C).

The distribution of Pt-LIS1 in the testis of *P. trituberculatus* during spermatogenesis was determined through IF experiments. The different types of spermatogenic cells were distinct by HE staining (Fig. 3DA4-G4). In spermatogonia, spermatocytes, and early spermatids, the nuclei are round in shape (Fig. 3DA4-D4). In mid-stage spermatids, the nuclei migrate to one side of the cell (Fig. 3DE4), while in late-stage spermatids, the nuclei gradually compress into a cup-shaped structure (Fig. 3DF4). In mature sperm, the spermatid nucleus undergoes further invagination, forming a cup-shaped nuclear cap (Fig. 3DG4). In spermatogonia, primary spermatocytes in the metaphase of meiosis I and secondary spermatocytes stage, Pt-LIS1 displayed uniform distribution in the perinuclear cytoplasm (Fig. 3DA1-C3). During early and mid-stage spermatids, Pt-LIS1 was observed in the perinuclear cytoplasm and around the proacrosomal vesicle (Fig. 3DD1-E3). In late spermatids, as the nucleus formed a cup shape, Pt-LIS1 signals concentrated in the subacrosomal space and acrosomal vesicles (Fig. 3DF1-F3). In mature sperm, Pt-LIS1 signals were also concentrated in the subacrosomal space and acrosomal tube (Fig. 3DG1-G3). The distribution of Pt-LIS1 continuously changes with nuclear deformation and acrosome formation, suggesting its potential involvement in these processes.

Colocalization of Pt-LIS1 and Pt-DHC, Pt-DIC, α-Tubulin, PHB and Acrosin during spermatogenesis in *P. trituberculatus*

To further investigate the function of the Pt-LIS1 protein in spermatogenesis in *P. trituberculatus*, we employed IF combined with laser confocal microscopy to explore the relationship between Pt-LIS1 and Pt-DHC, Pt-DIC, α-Tubulin, PHB and Acrosin.

LIS1 is an important regulator of Dynein-1, while Pt-DHC and Pt-DIC are important subunits of Dynein-1. Therefore, we detected the relationship between Pt-LIS1 and Pt-DHC(/Pt-DIC). The results demonstrated consistent colocalization of Pt-DHC and Pt-DIC with Pt-LIS1 during the spermatogenesis of *P. trituberculatus* (Figs. 4, 5). From spermatogonia to the early spermatid stage, Pt-DHC and Pt-DIC were distributed in the

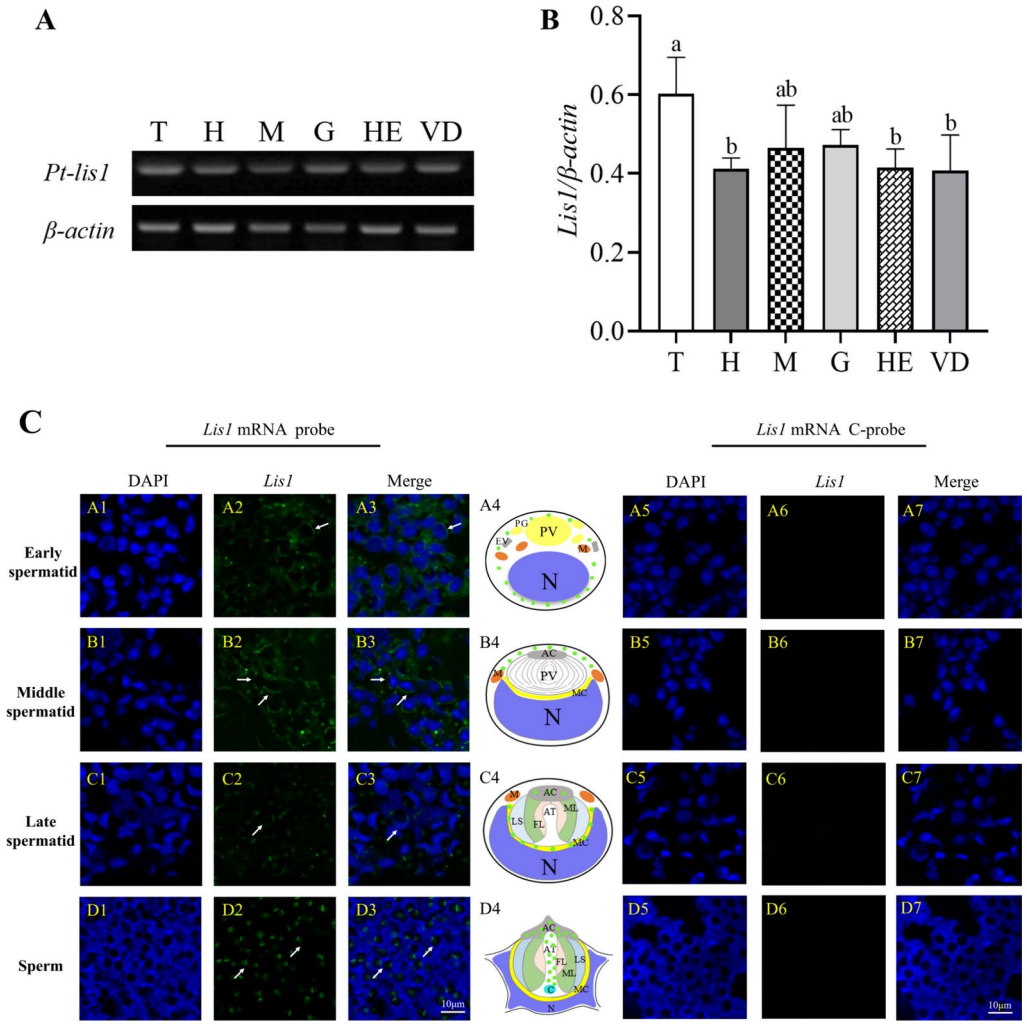

Fig. 2. The expression and distribution of *Pt-Lis1* mRNA in *P. trituberculatus*. (A) Semiquantitative PCR results of *Pt-Lis1* mRNA in different tissues of *P. trituberculatus*, the original blot is presented in Supplementary Fig. 1. (B) The gray value of semiquantitative PCR images was extracted by Image J, the expression of *Pt-Lis1* mRNA in the testis was the highest (different letters above columns indicate significant differences, $P < 0.05$). T: testis; H: heart; M: muscle; G: gill; HE: hepatopancreas; VD: vas deferens. (C) The spatial and temporal distribution of *Pt-Lis1* mRNA during spermiogenesis in *P. trituberculatus*. The left picture (A1-D3) shows the distribution of *Pt-Lis1* mRNA at different stages of spermiogenesis. The blue signal is the nucleus, and the green fluorescence is the *Pt-Lis1* mRNA signal. The arrow indicated that the typical signals of Pt-*Lis1*. (A1-A3) Early spermatid; (B1- B3) Middle spermatid; (C1-C3) Late spermatid; (D1-D3) Sperm; (A3-D3) Colocalization of *Pt-Lis1* mRNA with nuclear signals. The right picture (A5-D7) is a negative control (incubated with *Pt-Lis1* mRNA control probe) and did not detect signals other than DAPI, demonstrating the specificity of the *Pt-Lis1* mRNA probe. (A4-D4) The localization pattern of the *Pt-Lis1* mRNA signal in different stages of spermiogenesis was plotted according to the localization results. N: nuclear; AC: acrosome cap; AT: acrosome tube; MC: membrane complex; FL: fibrous layer; ML: intermediate layer; LS: lamellar structure; RA: radial arm. Scale bar = 10 μm.

cytoplasm around the nucleus and were highly colocalized with Pt-LIS1 (Fig. 4A1-D5, Fig. 5A1-C5). In the middle stage of spermatids, Pt-LIS1, Pt-DHC and Pt-DIC signals colocalized in the perinuclear cytoplasm, showing varying intensities between nucleus sides (Fig. 4E1-E5, Fig. 5D1-D5). Late spermatids exhibited strong Pt-LIS1 and Pt-DHC colocalization in the acrosomal cap and tube, with some signal in the subacrosomal space (Fig. 4F1-F5), while Pt-DIC signal was in the subacrosomal space and acrosomal tube (Fig. 5E1-E5). In mature sperm, Pt-DHC and Pt-DIC signals mainly concentrated in the inner nuclear cup and acrosomal tube, highly colocalized with Pt-LIS1 (Fig. 4G1-G5, Fig. 5F1-F5).

As Dynein-1 is a motor protein that moves along microtubules and Pt-LIS1 is an important regulator of Dynein-1, we examined the colocalization of Pt-LIS1 with α-Tubulin. Pt-LIS1 and α-Tubulin exhibited high colocalization during spermatogenesis (Fig. 6). In spermatogonia and spermatocytes, signals were uniformly distributed around the nucleus, with increased α-Tubulin intensity in spermatocytes (Fig. 6A1-B5). In early and middle stages of spermatids, Pt-LIS1 and α-Tubulin signals were colocalized in the perinuclear cytoplasm

(Fig. 6C1-D5). In late spermatids, both signals were colocalized in the acrosomal tube (Fig. 6E1-E5). In mature sperm, they were mainly clustered in the acrosomal tube and cap (Fig. 6F1-F5).

As Dynein-1 is involved in mitochondrial transport, we investigated the relationship between Pt-LIS1 and mitochondrial marker PHB. IF results revealed colocalization of Pt-LIS1 and PHB signals throughout spermatogenesis, evenly distributed around the nuclear in spermatogonia, spermatocytes, and early- and middle-stage of spermatids (Fig. 7A1-A5, B1-B5, C1-D5). In late spermatids, colocalization occurred in the acrosomal ducts (Fig. 7E1-E5), and in mature sperm, signals clustered in the acrosomal tubes and caps (Fig. 7F1-F5).

Acrosin, a crucial enzyme in crustacean sperm acrosomes, is transported along the microtubules by motor proteins. We investigated the relationship between Pt-LIS1 and Acrosin, finding colocalization in the cytoplasm around the nucleus in spermatogonia, early and middle stage of spermatids (Fig. 8A1-C5), and in mature sperm, colocalization occurred in the acrosomal cap and tube, with some Acrosin signals around the nucleus (Fig. 8D1-D5).

Detection of *Pt-Lis1* RNAi efficiency

To further explore the functions of Pt-LIS1 in the testis of *P. trituberculatus*, we performed an RNAi experiment by using dsRNA1 (with higher interference efficiency: 70%) (Fig. 9A, B). The mRNA and protein expression levels of Pt-LIS1 were significantly decreased in the *Pt-Lis1*-dsRNA group when compared to the control group, suggesting that Pt-LIS1 was silenced successfully (Fig. 9C-H).

Deficiency of *Pt-Lis1* in vivo affects both the expression level and distribution of Pt-DHC and Pt-DIC

Furthermore, we detected the expression of essential Dynein-1 subunits, finding a significant reduction in *Pt-dhc* and *Pt-dic* levels in the *Pt-Lis1*-dsRNA group (Fig. 10A-D). IF analysis revealed that the signals of Pt-DHC and Pt-DIC exhibited abnormal diffuse distributions in the cytoplasm in the *Pt-Lis1*-dsRNA group from spermatogonia to early spermatids (Fig. 10EA1-D5, FA1-C5). In the middle stage of spermatids, the signals were confined to one side of the nucleus in the *Pt-Lis1*-dsRNA group, whereas they evenly distributed around the entire nucleus in the control group (Fig. 10EE1-E5, FD1-D5). In late spermatids, the signals of Pt-DHC and Pt-DIC in the *Pt-Lis1*-dsRNA group were only weakly distributed within the acrosomal cap, exhibiting a decreased distribution within the subacrosomal space and acrosomal tube to that in the control group (Fig. 10EF1-F5, FE1-E5). In *Pt-Lis1*-dsRNA group, Pt-DHC and Pt-DIC signals were nearly undetectable compared to mature spermatids in the control group (Fig. 10EG1-G5, FF1-F5). Overall, these results indicate that *Pt-Lis1* knockdown disrupts Dynein-1 expression and distribution in *P. trituberculatus* testes. Statistical analysis further revealed a significant reduction in the number of spermatids with normal Pt-LIS1 and Pt-DHC (or Pt-DIC) signal distribution at each stage (Fig. 10G-N).

Deficiency of *Pt-Lis1* in vivo influences the expression level of related genes (*Pt-Nude*, *phb*, *p53* and *caspase-3*) in testes

The relative expression levels of related genes in the testis were analyzed by using *β-actin* and *gapdh* as double reference genes. In the *Pt-Lis1*-dsRNA group, the relative expression of *phb* was not significant changed (Fig. 11A, B), and the relative expression of *Pt-Nude* (another regulator of Dynein-1) in the testis was not significant changed (Fig. 11C, D). The expression of apoptosis genes (*p53* and *caspase-3*) in the testis was significantly increased (Fig. 11E-H).

Knockdown of *Pt-Lis1* leads to abnormal colocalization of Pt-LIS1 and α-Tubulin in the testis of *P. trituberculatus*

We further explored the relationship between Pt-LIS1 and α-Tubulin after *Pt-Lis1* silencing. Compared to the control group, colocalization signals of Pt-LIS1 and α-Tubulin were significantly weakened at all spermatogenesis stages (Fig. 12). From spermatogonia to early spermatids, α-Tubulin signal diffusely distributed in the perinuclear cytoplasm (Fig. 12A1-C5); in the middle stage of spermatids, α-Tubulin signaling was weakly distributed on one side of the nucleus (Fig. 12D1-D5); in late spermatids, α-Tubulin signaling was weakly distributed in acrosome (Fig. 12E1-E5); and in mature sperm, α-Tubulin signaling was observed only on the nucleus side (Fig. 12F1-F5).

Discussion

Structure Analysis of LIS1

Analyzing the structure of LIS1 is crucial for unraveling its functional roles and understanding its contributions to various cellular processes. In this study, we conducted a comprehensive structural analysis of LIS1, shedding light on its intricate composition and potential implications for cellular dynamics. LIS1 serves as a crucial regulator in Dynein-1-mediated cell development across different species[20,25–27]. Pt-LIS1 exhibits conserved domains, including the LISH domain at the N-terminus and a β-propeller domain at the C-terminus. The LISH domain, present in various proteins across the eukaryotic genome and associated with genetic syndromes[28], plays an essential role in LIS1 dimerization[29]. The β-propeller domain of LIS1 consists of multiple WD40 structural domains, which are characterized by highly conserved repeating units, and is implicated in assisting Dynein-1 in the transport of cellular cargoes along microtubules and the regulation of cell division[30]. The presence of these domains is consistent with previous findings in other species such as *Homo sapiens*, *Mus musculus*, and *Drosophila melanogaster*, and aligns with LIS1's known roles in cellular processes such as microtubule dynamics, intracellular transport, and cell division[31–33].

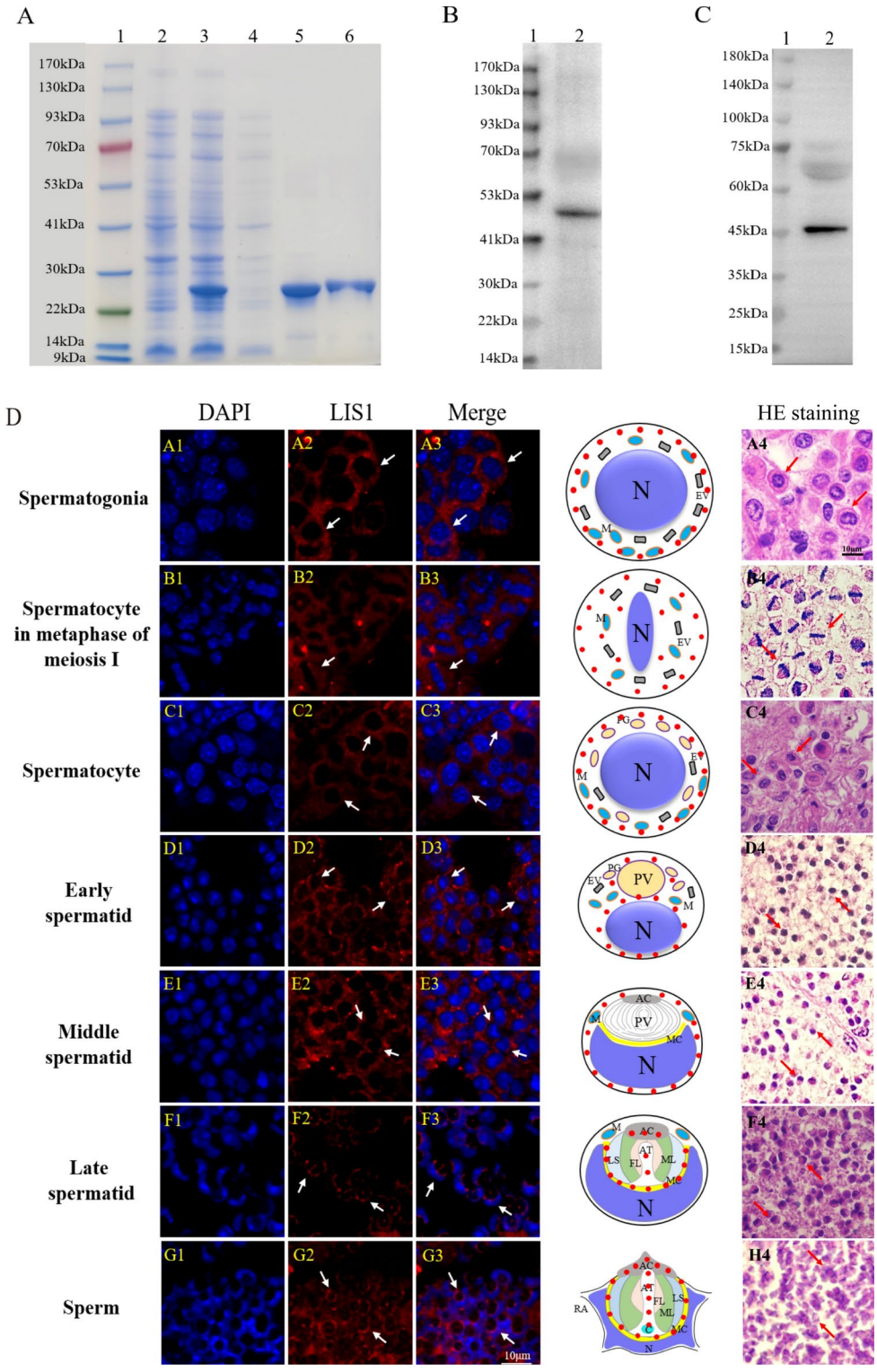

Pt-LIS1 was necessary for spermatogenesis in *P. trituberculatus*

Spermatogenesis is an indispensable part of sexual reproduction in animals, and spermatogonia undergo proliferation, differentiation and metamorphosis to form mature sperm[34]. Compared to other species, the mature sperm of crustaceans have a more specialized morphology, with nonmotile tailless sperm[5,6]. Understanding the pivotal role of Pt-LIS1 in spermatogenesis is crucial for unraveling the intricate process of sperm development in *P. trituberculatus*. Our investigation examining the pattern of *Pt-Lis1* mRNA and protein throughout the various stages of spermatogenesis firstly. We observe robust expression of *Pt-Lis1* in multiple tissues, with the highest levels found in the testis, indicating its significant involvement in sperm development. This finding indicates that the regulatory factor *Pt-Lis1* plays an equally crucial role in sperm development and spermatogenesis as Dynein-1 in *P. trituberculatus*, a viewpoint consistent with Mesngon et al.[23].

◀**Fig. 3**. Verification of the Pt-LIS1 antibodies and the localization and distribution of Pt-LIS1 protein during spermatogenesis. (**A**) Coomassie blue staining was used to detect the recombinant Pt-LIS1 protein obtained by prokaryotic expression. Lane 1: Marker; lane 2: no induced bacterial liquid; lane 3: 1 mM IPTG induced expression of bacterial solution; lane 4: the supernatant of the induced expression bacterial liquid; lane 5: precipitation of induced expression bacteria; lane 6: Purified Pt-LIS1 recombinant protein. (B) Rabbit-specific antibody against Pt-LIS1 was verified by WB. (C) Rat-specific antibody against Pt-LIS1 was verified by WB, the original blot is presented in Supplementary Fig. 2. (D) The localization and distribution of Pt-LIS1 protein during spermatogenesis. (A1-A4) Spermatogonia; (B1-B4) Primary spermatocytes in metaphase of meiosis I; (C1-C4) Secondary spermatocyte; (D1-D4) Early spermatid; (E1-E4) Middle spermatid; (F1-F4) Late spermatid; (G1-G4) Mature sperm. (A4-G4) HE staining of different types of spermatogenic cells. The blue color indicates the nuclei stained with DAPI; the red color indicates Pt-LIS1; the arrows indicated that the typical signals of Pt-LIS1. N: nuclear; AC: acrosome cap; AT: acrosome tube; MC: membrane complex; FL: fibrous layer; ML: intermediate layer; LS: lamellar structure; RA: radial arm. Scale bar = 10 μm.

Our analysis demonstrates that Pt-LIS1 exhibits dynamic distribution patterns throughout spermatogenesis, with particularly notable changes during the stages of nuclear deformation and acrosome formation. Pt-LIS1 is uniformly distributed in the perinuclear cytoplasm of spermatogonia and spermatocytes, suggesting its potential involvement in both mitosis of spermatogonia and meiosis of spermatocyte. This aligns with previous studies in *Drosophila* embryos[35] and HeLa cells[36], indicating the essential role of LIS1 in mitosis and meiosis regulation. During the transition from early to late spermatids, the Pt-LIS1 mRNA and protein signal exhibited dynamic changes in response to nuclear morphology alterations, hinting at its potential involvement in nuclear deformation. Additionally, as spermatids matured into sperm, *Pt-Lis1* signaling gradually concentrated in the subacrosomal space, acrosomal tube and cap, suggesting its association with acrosome formation. These observations align with previous research by Nayernia et al.[22], which highlighted the crucial role of LIS1 in acrosome formation and its structural integrity during mouse spermatogenesis.

Pt-LIS1 regulates Dynein-1 transport along microtubule and affects microtubule assembly

Dynein-1 plays a crucial role in regulating diverse cellular processes, including spermatogenesis and oogenesis[37], organelle translocation[38], spindle assembly[39,40], and nuclear translocation[41], and relies on microtubules to facilitate the transport of cellular cargo to its designated location for proper functioning. Notably, Dynein-1 has been shown only dependent on microtubules[42]. Microtubules, integral components of the cytoskeleton found in nearly all eukaryotes, consist of heterodimers of α-Tubulin and β-Tubulin[43]. Our colocalization analysis demonstrates the extensive overlap between Pt-LIS1 and α-Tubulin throughout spermatogenesis, supporting Pt-LIS1's role as a regulator of Dynein-1 in transporting cellular cargo along microtubules, consistent with previous findings[26]. Furthermore, the signals of Pt-LIS1 and α-Tubulin exhibit a diffuse distribution, with weakened colocalization observed following *Pt-Lis1* knockdown (Fig. 12). Considering Dynein-1's role in microtubule formation[15], the knockdown of *Pt-Lis1* seems to result in the diffused distribution of α-Tubulin, indicating that Pt-LIS1 affect microtubule assembly.

The transport of cellular cargoes along microtubules is a fundamental process essential for various cellular functions[44]. PHB (prohibitin) is a vital inner mitochondrial membrane protein, and recognized as a marker for mitochondria [45–47]. Studies have highlighted PHB's expression and functional significance in animal spermatogenesis[48,49]. In *P. trituberculatus* spermatogenesis, PHB colocalizes with Pt-DHC, a Dynein-1 subunit involved in mitochondrial transport[16]. Investigating the Pt-LIS1 and mitochondria relationship, we focus on Pt-LIS1 colocalization with PHB. The observed colocalization throughout spermatogenesis suggests LIS1's involvement in regulating Dynein-1-mediated mitochondrial transport. Additionally, Pt-LIS1 may contribute to Dynein-1-mediated enzymatic transport in spermatogenesis. Acrosin, a trypsin-like serine protease specific to the sperm acrosome, is crucial for the acrosome reaction, penetration of the zona pellucida during sperm-egg binding, and release of other enzymes enhancing sperm motility[50,51], and a previous study showed that motor proteins transport Acrosin along the acrosome[9]. Colocalization of Pt-LIS1 and Acrosin in the acrosome tube and acrosome cap suggesting that Pt-LIS1 may be involved in enzyme transport during spermatogenesis.

Pt-LIS1 plays an important role in the expression of the Dynein −1 subunit

Dynein-1 primarily binds to microtubules via the heavy chain Pt-DHC and attaches to cargo primarily through the intermediate chain Pt-DIC. Consequently, Pt-DHC and Pt-DIC were chosen as the target proteins for colocalization analysis[52]. Our findings indicate that Pt-LIS1 knockdown significantly reduces the expression levels of *Pt-dhc* and *Pt-dic* in the testis, key components of the Dynein-1 complex. This suggests that that Pt-LIS1 regulates Dynein-1 subunits at the transcriptional level, impacting the function of Dynein-1. Our immunofluorescence and co-localization analyses reveal that *Pt-Lis1* knockdown leads to a reduction in the co-localization signal between Pt-LIS1 and Pt-DHC, as well as between Pt-LIS1 and Pt-DIC. Additionally, an increased number of spermatids exhibit abnormal distribution of colocalization signals (Fig. 10G-N), implying that *Pt-Lis1* absence may influence nuclear deformation and acrosome formation in *P. trituberculatus*. This observation aligns with the studies on mouse testes, where *Lis1* deletion resulted in spermatogenesis failure[22]. The pivotal role of Pt-LIS1 in modulating Dynein-1 expression and function underscores its significance in cellular dynamics and highlights its potential as a target for further investigation into the regulatory mechanisms governing cellular transport and organization.

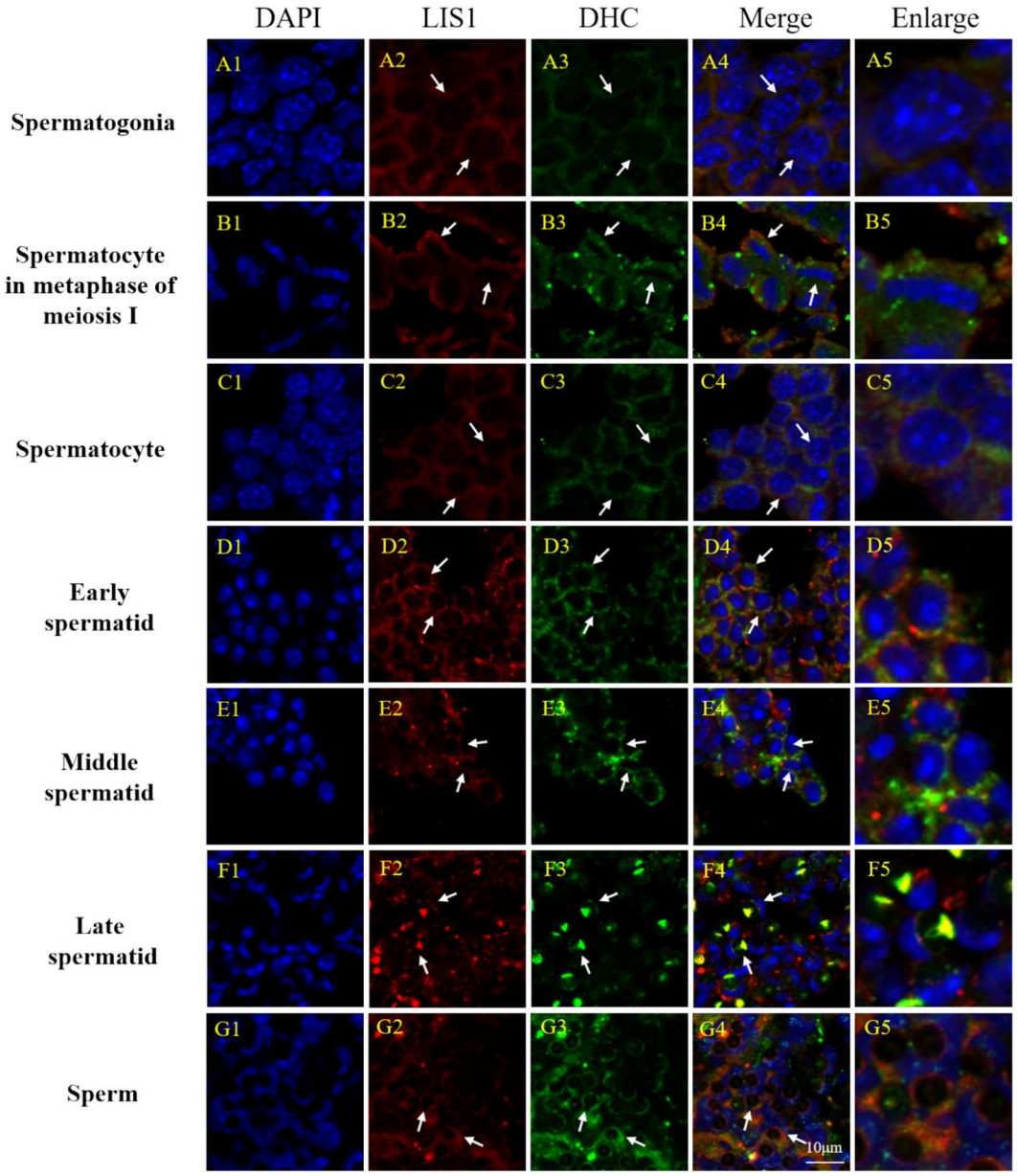

Fig. 4. Colocalization distribution of Pt-LIS1 and Pt-DHC proteins during spermatogenesis. (A1-A5) Spermatogonia; (B1-B5) Primary spermatocytes in metaphase of meiosis I; (C1-C5) Secondary spermatocyte; (D1-D5) Early spermatid; (E1-E5) Middle spermatid; (F1-F5) Late spermatid; (G1-G5) Mature sperm. The blue color indicates the nuclei stained with DAPI; the red color indicates Pt-LIS1; the green color indicates Pt-DHC; and the arrows indicated that the typical signals of Pt-LIS1 and Pt-DHC. N: nuclear; AC: acrosome cap; AT: acrosome tube; MC: membrane complex; FL: fibrous layer; ML: intermediate layer; LS: lamellar structure; RA: radial arm. Scale bar = 10 μm.

Pt-LIS1 as a key regulator of Dynein-1 in spermatogenesis of *P. trituberculatus*

Dynein-1 plays an important role in reproductive development in males[53–55]. Previous studies have demonstrated the necessity of motor proteins like Kinesin and Dynein-1 in sperm metamorphosis and acrosome formation during crustacean spermatogenesis[16,56]. Furthermore, the indispensable role of Dynein-1 has been firmly established in various cellular processes, including spermatogenesis and acrosome formation in *P. trituberculatus*[16,17]. Through colocalization analysis using IF and laser confocal microscopy techniques, we observed significant colocalization of Pt-LIS1 with Pt-DHC and Pt-DIC throughout different stages of spermatogenesis, including spermatogonia, spermatocytes, spermatids, and mature sperm. These results imply a close functional relationship between Pt-LIS1 and Dynein-1 in coordinating cellular processes during spermatid development. The intricate interplay between Pt-LIS1 and Dynein-1 underscores the complexity of microtubule dynamics and intracellular transport mechanisms. While our study focuses on the interaction between Pt-

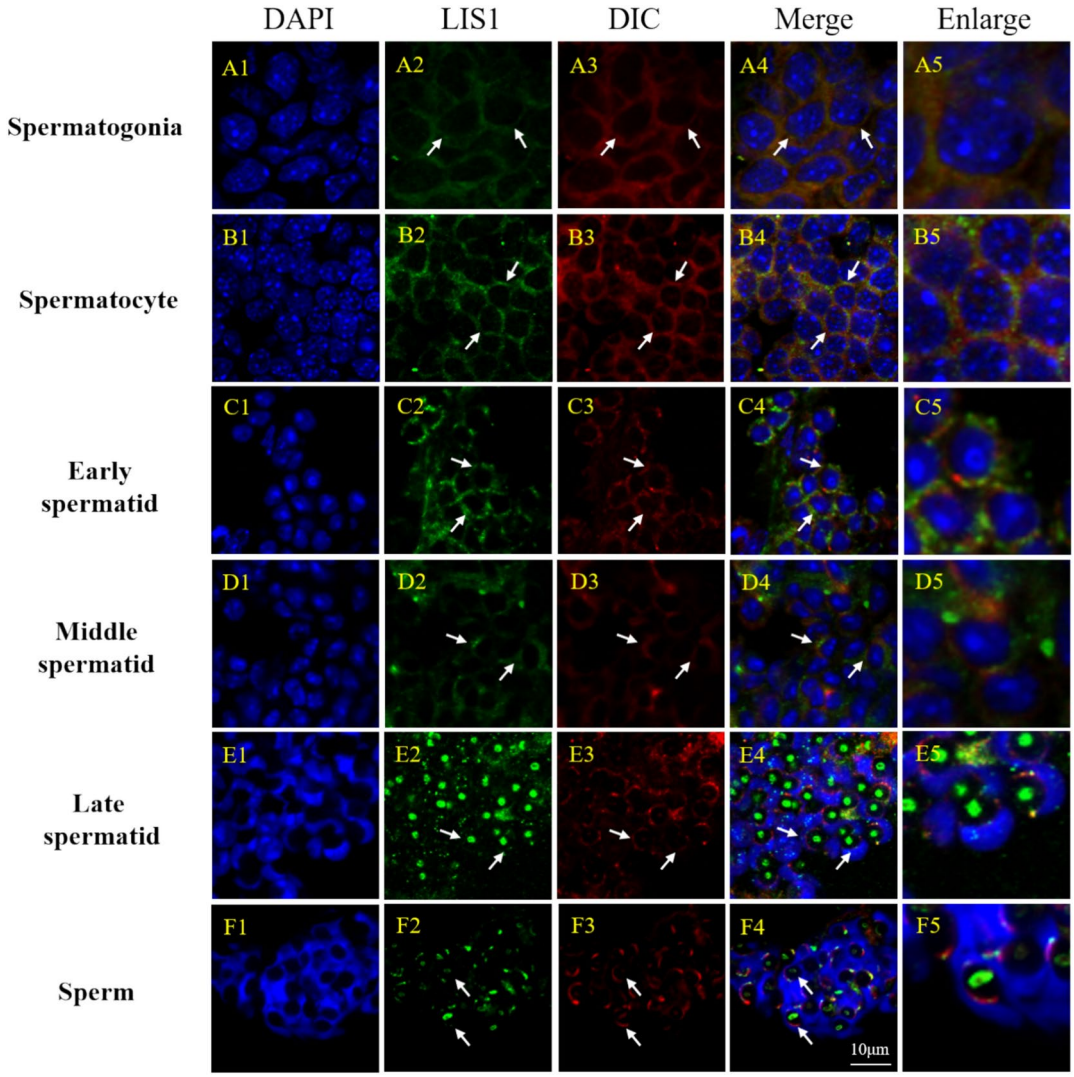

Fig. 5. Colocalization distribution of Pt-LIS1 and Pt-DIC proteins during spermatogenesis. (A1-A5) Spermatogonia; (B1-B5) Secondary spermatocytes; (C1-C5) Early spermatids; (D1-D5) Middle spermatids; (E1-E5) Late spermatids; (F1-F5) Mature sperm. The blue color indicates the nuclei stained with DAPI; the green color indicates Pt-LIS1; the red color indicates Pt-DIC; and the arrows indicated that the typical signals of Pt-LIS1 and Pt-DIC. N: nuclear; AC: acrosome cap; AT: acrosome tube; MC: membrane complex; FL: fibrous layer; ML: intermediate layer; LS: lamellar structure; RA: radial arm. Scale bar = 10 μm.

LIS1 and Dynein-1, further research is needed to elucidate the precise regulatory mechanisms governing their collaboration and its implications for spermatogenesis.

The intricate interplay between different regulatory factors within the Dynein complex highlights the complexity of cellular processes involving microtubule dynamics and intracellular transport[15,22]. The relationship between *Lis1* and *Nude* has been previously explored in various biological contexts, and studies have reported that *Lis1* can interact with *Nude* to regulate Dynein function[57]. Our findings indicate that *Pt-Nude* may not be directly influenced by *Pt-Lis1* expression levels or the associated knockdown. The lack of significant alteration in *Pt-Nude* expression post *Pt-Lis1* knockdown suggests a potential independence in the regulatory mechanisms governing these two Dynein-associated factors. However, there is no clear studies on the combination of the two and the regulatory mechanisms.

Moreover, our study provides insights into the potential involvement of Pt-LIS1 in mitochondrial function, apoptosis regulation, and maintenance of spermatogenic cell viability. The expression of *phb* did not show significant changes. However, further investigation is needed to determine whether *Pt-Lis1* affects mitochondrial morphology and function. P53, as a critical tumor suppressor, is activated in response to various stress signals, thereby orchestrating various cellular processes such as cellular senescence, metabolism, apoptosis, and DNA repair[58]. The expression level of *p53* can serve as an indicator of the degree of cellular stress[59]. *Caspase-3* a pivotal gene in apoptosis, is implicated in the pathogenesis of neurodegenerative diseases, and its overactivation has emerged as a potential therapeutic target for apoptosis-related[60]. Nayernia et al. (2003) reported that reduced Pt-LIS1 expression led to impaired spermatogenesis in mice, while Sitaram et al. (2012) demonstrated that Pt-*Lis1*

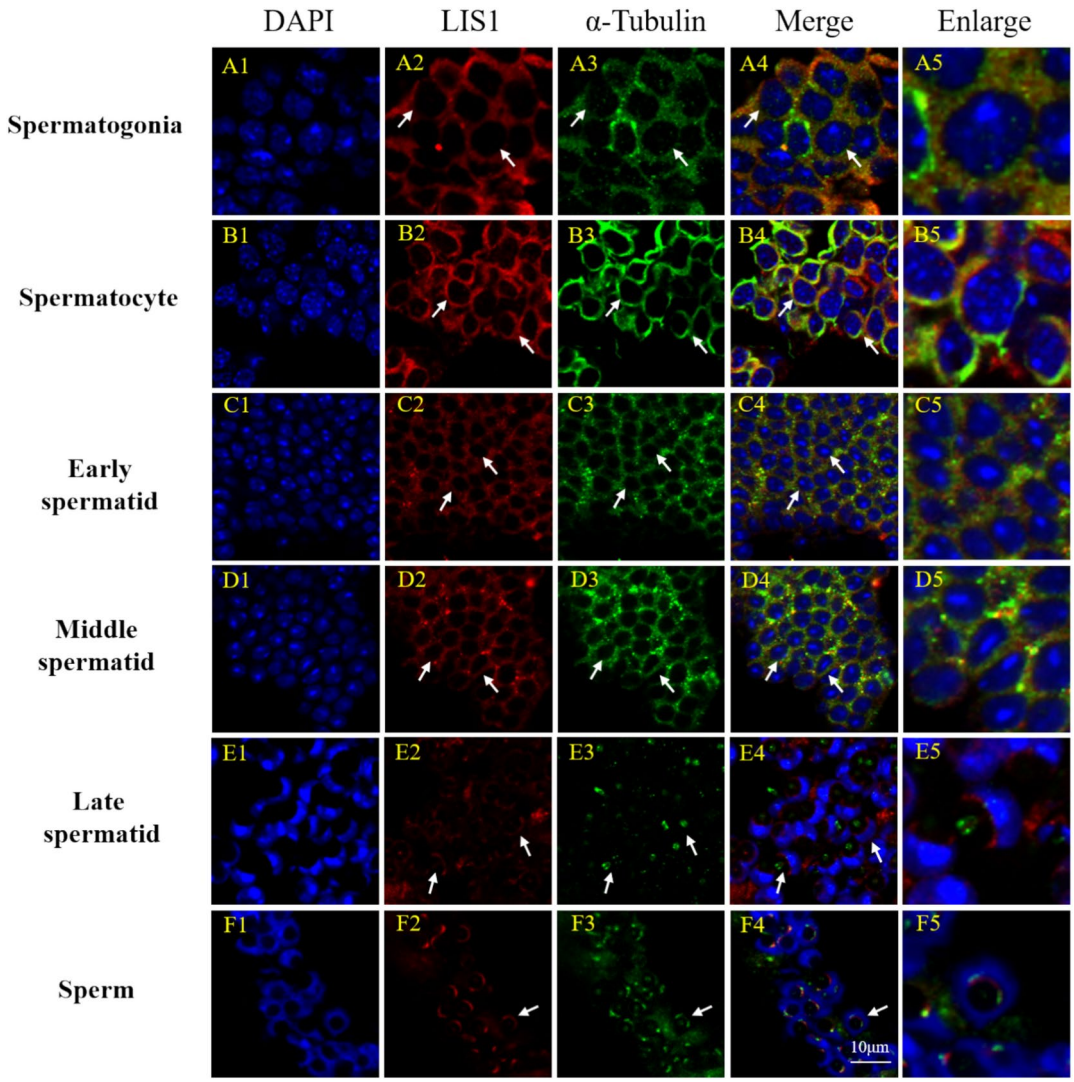

Fig. 6. Colocalization distribution of Pt-LIS1 and α-Tubulin proteins during spermatogenesis. (A1-A5) Spermatogonia; (B1-B5) Secondary spermatocytes; (C1-C5) Early spermatids; (D1-E5) Middle spermatids; (E1-E5) Late spermatids; (F1-F5) Mature sperm. The blue color indicates the nuclei stained with DAPI; the red color indicates Pt-LIS1; the green color indicates α-Tubulin and the arrows indicated that the typical signals of Pt-LIS1 and α-Tubulin. N: nuclear; AC: acrosome cap; AT: acrosome tube; MC: membrane complex; FL: fibrous layer; ML: intermediate layer; LS: lamellar structure; RA: radial arm. Scale bar = 10 μm.

deletion in *Drosophila* resulted in abnormal spermatogonial division and compromised male spermatogenesis. The observed upregulation of *p53* and *caspase-3* expression subsequent to *Pt-Lis1* knockdown indicates a role for Pt-LIS1 in modulating spermatogenic cell apoptosis. Spermiogenesis, as the final stage of spermatogenesis, is crucial for proper sperm formation. Reduced expression of *Lis1* during this stage may lead to excessive apoptosis of spermatogenic cells, which could significantly impair sperm maturation. Therefore, we speculate that Pt-LIS1 may play a crucial role in maintaining the survival of spermatogenic cells and ensuring the quantity of both spermatogenic cells and sperm. But we need to conduct further discussions regarding the extent of apoptosis in spermatogenic cells.

Conclusions

In summary, our study revealed that *Pt-Lis1* exhibited high expression levels in the testis, predominantly localized around the nucleus and in the developing acrosome during spermatogenesis (Fig. 13). The localization suggests potential involvement of Pt-LIS1 in mitosis and meiosis, as well as participation in nuclear deformation and acrosome formation processes. After *Pt-Lis1* knockdown, we observed decreased expression of Pt-*dhc* and Pt-*dic*, accompanied by aberrant colocalization patterns between Pt-LIS1 and Pt-DHC, Pt-DIC, α-Tubulin, PHB, and Acrosin. These findings imply that Pt-LIS1 acts as a crucial regulator ensuring proper Dynein-1-mediated cargo transport along microtubules. Moreover, the upregulation of apoptosis-related genes, *p53* and *caspase-3*, following *Pt-Lis1* knockdown suggests its potential involvement in regulating spermatogenic cell apoptosis in

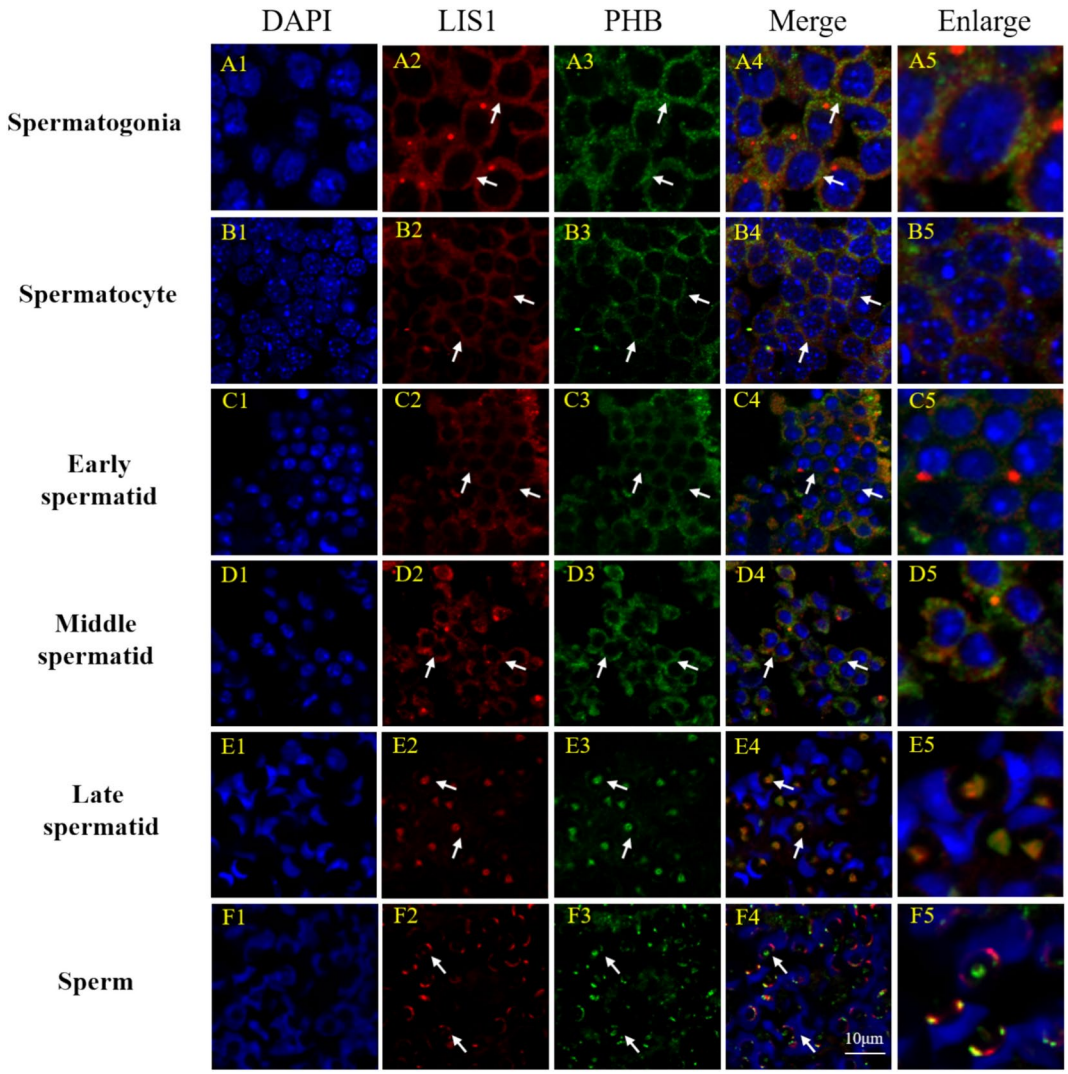

Fig. 7. Colocalization distribution of Pt-LIS1 and PHB proteins during spermatogenesis. (A1-A5) Spermatogonia; (B1-B5) Secondary spermatocytes; (C1-C5) Early spermatids; (D1-D5) Middle spermatids; (E1-E5) Late spermatids; (F1-F5) Mature sperm. The blue color indicates the nuclei stained with DAPI; the red color indicates Pt-LIS1, the green color indicates PHB and the arrows indicated that the typical signals of Pt-LIS1 and PHB. N: nuclear; AC: acrosome cap; AT: acrosome tube; MC: membrane complex; FL: fibrous layer; ML: intermediate layer; LS: lamellar structure; RA: radial arm. Scale bar = 10 μm.

P. trituberculatus, suggesting that Pt-LIS1 plays an important role in maintaining the survival of spermatogenic cells and ensuring the number of spermatogenic cells.

Materials and methods

Experimental animals

The study was conducted on 70 mature male and active *P. trituberculatus* crabs sampled from the Xianxiang Jiandao aquaculture farm (Ningbo, China). All crabs had free access to food with 12:12 h of light/dark cycle and constant environmental conditions (24–26 °C, 25‰ salinity in water) before experimentation and thereafter. Two male New Zealand white rabbits were purchased from Jianfei Experimental Rabbit Farm, Simen Town, Yuyao, Ningbo (SCXK (Zhejiang) 20,220,002) and fed in separate cages at the Experimental Animal Center of Ningbo University (SYXK (Zhejiang) 2019–0005). Four male SD rats were purchased from Zhejiang Viton Lihua Laboratory Animal Technology Co., Ltd. (SCXK (Zhejiang) 2024–0001), and fed in separate cages at the Ningbo University Laboratory Animal Center (SYXK (Zhejiang) 2019–0005). All rabbits and rats had free access to food and water with 12:12 h of light/dark cycle and constant environmental conditions before experimentation and thereafter.

Ethical statement.

All experiments were pursued by the standards of the requirements of the governing regulation for the use of experimental animals in Zhejiang Province (Zhejiang provincial government order No. 263, released on17 August 2009, effective from 1 October 2010) and were performed after the approval of the Animal Care and

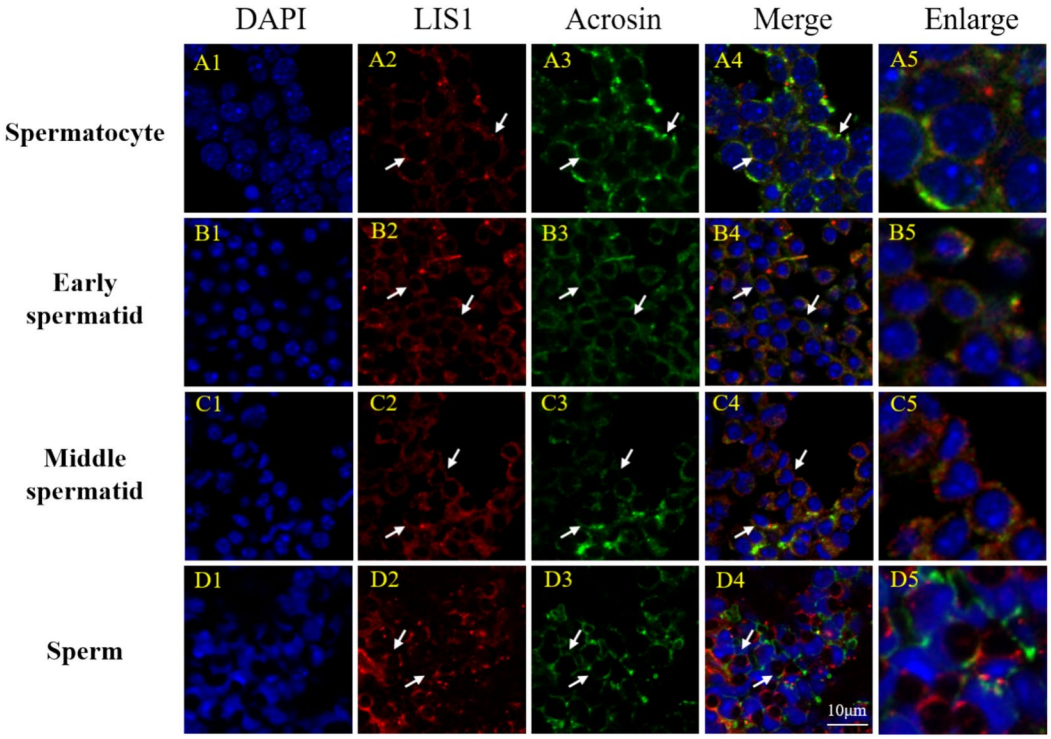

Fig. 8. Colocalization distribution of Pt-LIS1 and Acrosin proteins during spermatogenesis.(A1-A3) Secondary spermatocytes; (B1-B5) Early spermatids; (C1-C5) Middle spermatids; (D1-D5) Mature sperm. The blue color indicates the nuclei stained with DAPI; the red color indicates Pt-LIS1; the green color indicates Acrosin and the arrows indicated that the typical signals of Pt-LIS1 and Acrosin. N: nuclear; AC: acrosome cap; AT: acrosome tube; MC: membrane complex; FL: fibrous layer; ML: intermediate layer; LS: lamellar structure; RA: radial arm; Scale bar = 10 μm.

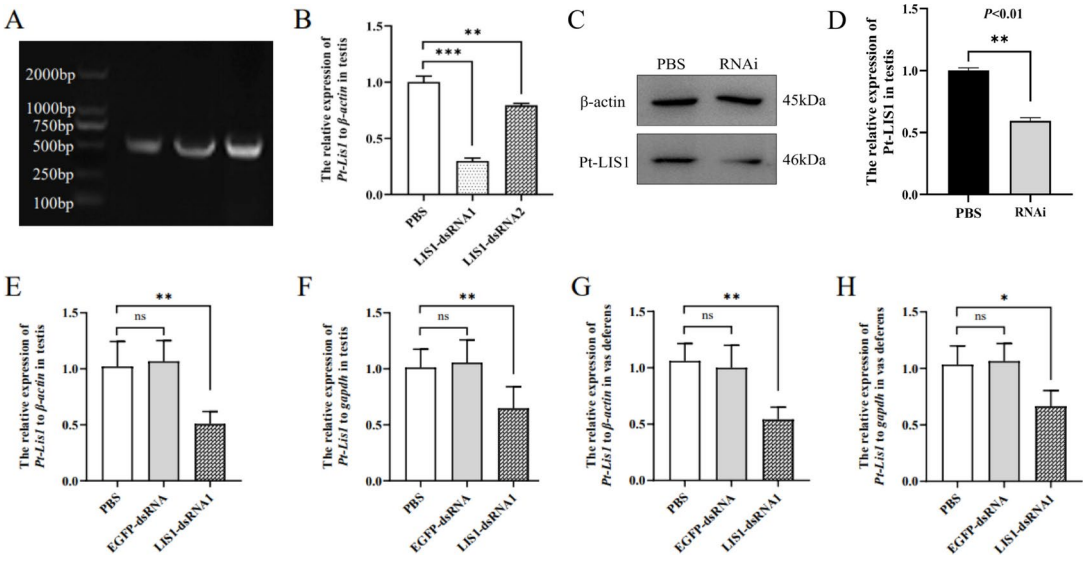

Fig. 9. Knockdown efficiency of *Pt-Lis1* by dsRNA injection in vivo. (**A**) Synthesis of specific dsRNA, *egfp*-dsRNA (463 bp), *Pt-Lis1*-dsRNA1 (435 bp) and *Pt-Lis1*-dsRNA2 (441 bp), the original blot is presented in Supplementary Fig. 4. (B) The results of qPCR showed that the relative expression of *Pt-Lis1* mRNA was significantly decreased after dsRNA interference. (C) WB detection of Pt-LIS1 expression in the testis, original blots are presented in Supplementary Fig. 5, 6. (D) ImageJ software was used to extract the grayscale values of the protein bands, and Pt-LIS1 protein expression was significantly reduced after interference with *Pt-Lis1*. (E–H) The relative expression of *Pt-Lis1* mRNA in the testis and vas deferens was significantly reduced. "ns" means no significant difference, $P > 0.05$, "*" means a significant difference, $P < 0.05$, "**" means an extremely significant difference, $P < 0.01$.

Use Committee of Ningbo University and the Animal Ethics and Welfare Committee of Ningbo University (approval number NBU20220155). All procedures were designed following the ARRIVE guidelines (PLoS Bio 8(6), e1000412, 2010) and conducted in accordance with the eighth edition (2011) of the rules for the care and use of laboratory animals.

Synthesis of dsRNA

Primers carrying the T7 promoter sequence were designed by Primer Premier 5.0 software (Supplementary Table 1). Fragments were cloned by PCR using the following procedure: 1 cycle at 94 °C for 5 min, 8 cycles at 94 °C for 30 s, 62 °C for 30 s (decrease rate 0.5 °C/cycle), and 72 °C for 30 s, 27 cycles at 94 °C for 30 s, 58 °C for 30 s, and 72 °C for 30 s, and then a final extension at 72 °C for 10 min. The PCR product was used as the template to synthesize dsRNA according to the TranscriptAid T7 High Yield Transcription Kit instructions (Thermo Scientific, Shanghai, China).

Experimental design

Crabs were classified into the following groups: Control group: consisted of 25 healthy male crabs that had not received any type of treatment, PBS group: consisted of 15 male crabs which were injected with 2 μL/g RNase-free PBS (injected once every 48 h into the fifth pleopod, for a total of 5 injections), *Pt-Lis1*-dsRNA1 group: consisted of 15 male crabs which were injected with 2 μg/g *Pt-Lis1*-dsRNA1 dilution liquid (injected once every 48 h into the fifth pleopod, for a total of 5 injections), *Pt-Lis1*-dsRNA2 group: consisted of 6 male crabs which were injected with 2 μg/g *Pt-Lis1*-dsRNA2 dilution liquid (injected once every 48 h into the fifth pleopod, for a total of 5 injections), *egfp*-dsRNA group: consisted of 9 male crabs which were injected with 2 μg/g *egfp*-dsRNA dilution liquid (injected once every 48 h into the fifth pleopod, for a total of 5 injections). All crabs followed a regimen of moderate exercise that reproduced an active lifestyle.

Collection of samples

Crabs were dissected on ice, and five tissues (testis, muscle, gill, hepatopancreas and vas deferens) were detached, immediately frozen in liquid nitrogen, and stored at −80 °C for total RNA and protein extraction. Additionally, some testis sections were fixed in 4% paraformaldehyde in 0.1 M PBS for FISH and IF experiments.

Antigen immunization injections

According to the amino acid sequence of Pt-LIS1 and the antigen site online prediction website, the specific region was selected as the antigen fragment (encoding 212 amino acids, approximately 28.87 kDa), and then the primers were designed (BamH1 and Xho1 cut sites were added at the two ends of the Pt-LIS1 fragment, respectively, YH-LIS1-F/R). The cloned correct DNA fragment was subjected to a double digestion reaction with plasmid pET28-a (+) (provided by the sperm laboratory of Zhejiang University) and then ligated with T4 ligase (Takara, Beijing, China). Through transformation and sequencing, the correct plasmid was extracted using the Plasmid Extraction Mini Kit (OMEGA, Guangzhou, China). The correct recombinant plasmid was transferred into DE3 competent cells and inoculated into 10 mL $Kana^+$ liquid medium to expand the culture (37 °C, 220 g). When the OD value reached 0.4–0.6, 1 mM IPTG solution was added to induce recombinant protein expression (37 °C, 220 g, 6 h). The bacterial solution was resuspended after sedimentation, ultrasonically crushed, and centrifuged (10,000 g, 4 °C, 15 min). Purification of inclusion body proteins from precipitates was performed using a His-tagged protein purification kit (Beyotime, Shanghai, China) according to the manufacturer's instructions. After identification by SDS-PAGE, the purified recombinant protein was loaded into a dialysis bag for renaturation with a linear 6, 4, 2, 1, and 0 M urea gradient in the dialysate for 8 h. Finally, the protein concentration was detected by using the Super-Bradford Protein Quantification Kit (Beyotime, Shanghai, China).

The purified recombinant protein was fully mixed with Freund's complete adjuvant at the first immunization injection. Then, each SD rat was injected subcutaneously with 400 μg recombination protein, and each New Zealand rabbit was injected with 600 μg recombination protein. At the 2nd-5th immunization injection (once every other week), the purified Pt-LIS1 recombinant protein was fully mixed with Freund's incomplete adjuvant, each SD rat was injected with 200 μg recombination protein, and each New Zealand rabbit was injected with 300 μg recombination protein. All rats were overnight fasting, and blood samples were collected from the retro-orbital vein under deep anesthesia using isoflurane (inhalation 100%), the rats were then euthanized via cervical dislocation. All rabbits were anesthetized using isoflurane, and blood samples were collected from the ear vein. The rabbits were then euthanized via auricular vein air injection.

Full-length cDNA cloning of *Pt-Lis1*

Total RNA was extracted from testes by using TRIzol Reagent (Invitrogen, USA). According to the manufacturer' instructions, the obtained RNA was used for normal reverse transcription using the Prime-Script® RT Reagent Kit (Takara, Dalia, China). A SMARTer RACE 5′/3′ Kit (Takara, Dalian, China) was used to synthesize 3′ and 5′ terminal cDNA from the testis of *P. trituberculatus*. The reverse transcribed products (cDNA) were stored at −20 °C for subsequent PCR.

We obtained the *Pt-Lis1* cDNA sequence of *Drosophila melanogaster* (GenBank accession no. NM_001259432.2) from the National Center for Biotechnology Information (https://www.ncbi.nlm.nih.gov/, NCBI) database and compared it with the genome of *P. trituberculatus*, subsequently obtaining the specific fragment. The sequence was imported into Primer Premier 5 software (Premier Biosoft International, Palo Alto, CA, USA) for the design of degenerate primers and sent to Youkang Biotechnology Co., Ltd. (Zhejiang, Hangzhou, China) for synthesis. The testis cDNA of *P. trituberculatus* was used as a template, and the Touchdown PCR (TD-PCR) program was

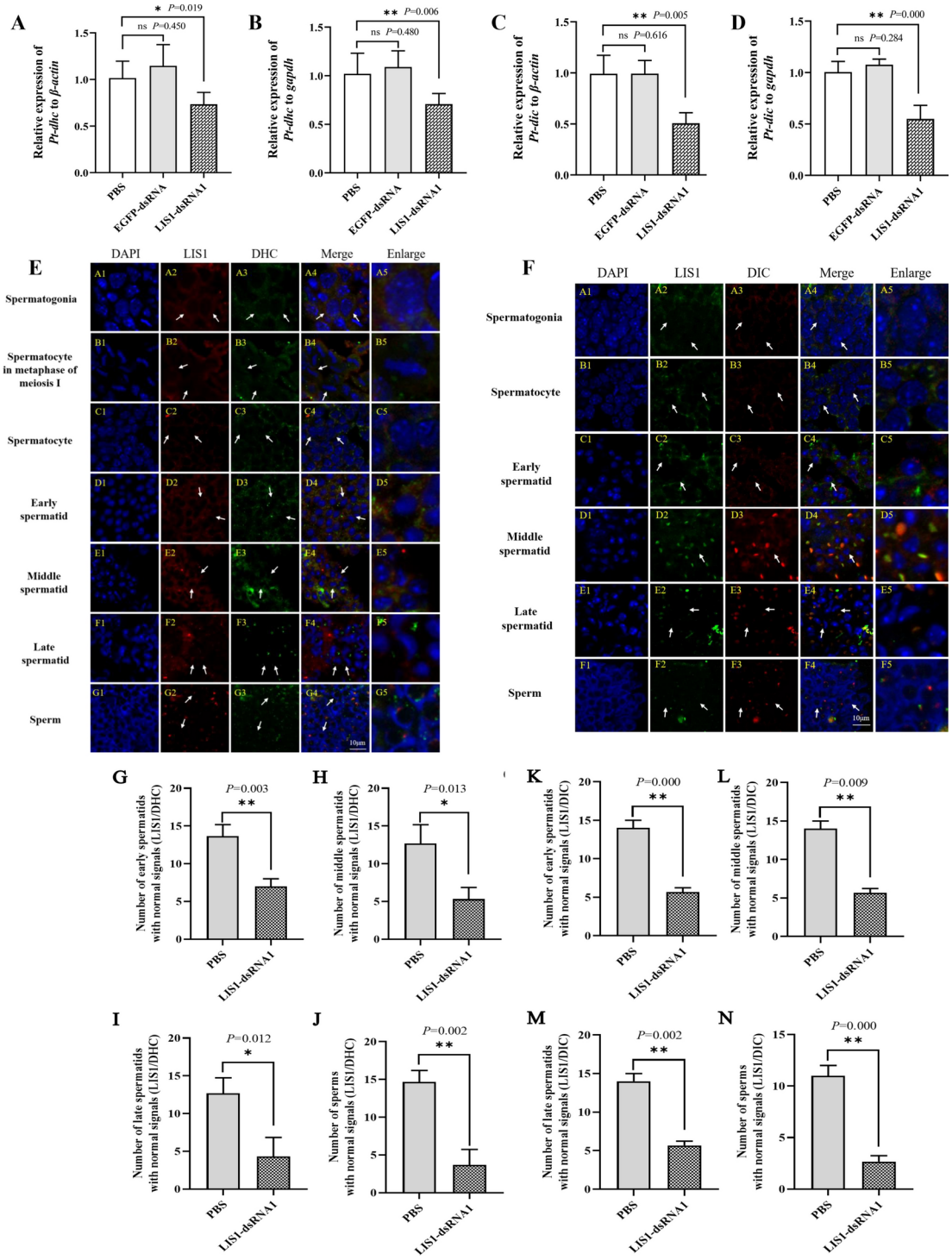

used to amplify the intermediate fragments of *Pt-Lis1*. TD-PCR was conducted as follows: 94 °C for 5 min; 8 cycles of 94 °C for 30 s, 55 °C for 30 s (decreased by 0.5 °C/cycle) and 72 °C for 45 s; 27 cycles of 94 °C for 30 s, 53 °C for 30 s, 72 °C for 45 s; and 72 °C for 10 min for the final extension. Then, we designed specific primers by using Primer Premier 5.0 software for RACE. The touch-down PCR used for 3′/5′ RACE was conducted as follows: 94 °C for 5 min; 8 cycles of 94 °C for 30 s, 72/71 °C for 30 s (decreased by 0.5 °C/cycle) and 72 °C for 1 min; 27 cycles of 94 °C for 30 s, 68/67 °C for 30 s and 72 °C for 1 min; and then a final extension at 72 °C for 10 min. These PCR products were separated, identified, and sequenced based on the method described by Chang et al.[9]. We assembled the intermediate segment and the clonal 3′ and 5′ cDNA segment sequences and obtained the full-length cDNA of *Pt-Lis1*. All primers used in the study are presented in Supplementary Table 2.

◀**Fig. 10**. Deficiency of *Pt-Lis1* in vivo affects the expression level and distribution of Pt-DHC and Pt-DIC. (**A**, **B**) The relative expression of *Pt-dhc* in the testis decreased; (**C**, **D**) The relative expression of *Pt-dic* in the testis was significantly decreased; (E) IF analysis revealed that the signals of Pt-LIS1 and Pt-DHC exhibited abnormal diffuse distributions in the cytoplasm in the Pt-*Lis1*-dsRNA group. (A1-A5) Spermatogonia; (B1-B5) Primary spermatocytes in the metaphase of meiosis I; (C1-C5) Secondary spermatocytes; (D1-D5) Early spermatids; (E1-E5) Middle spermatids; (F1-F5) Late spermatids; (G1-G5) Mature sperm, the Pt-DHC signal was nearly undetectable compared to control group. The blue color indicates the nuclei stained with DAPI; the red color indicates Pt-LIS1; the green color indicates Pt-DHC and the arrows indicated that the typical signals of Pt-LIS1 and Pt-DHC. (F) Colocalization of Pt-LIS1 and Pt-DIC proteins during spermatogenesis was diminished after *Pt-Lis1* silencing in vivo (A1-A5) Spermatogonia; (B1-B5) Secondary spermatocytes; (C1-C5) Early spermatids; (D1-D5) Middle spermatids, Pt-DIC signal was confined to one side of the nucleus, whereas it evenly distributed around the entire nucleus in the control group; (E1-E5) Late spermatids, Pt-DIC signal exhibit a decreased distribution within the subacrosomal space and acrosomal tube to that in the control group; (F1-F5) Mature sperm, the Pt-DIC signal was nearly undetectable compared to control group. The blue color indicates the nuclei stained with DAPI; the green color indicates Pt-LIS1; the red color indicates Pt-DIC, and the arrows indicated that the typical signals of Pt-LIS1 and Pt-DIC. N: nuclear; AC: acrosome cap; AT: acrosome tube; MC: membrane complex; FL: fibrous layer; ML: intermediate layer; LS: lamellar structure; RA: radial arm. (G-J) Number of spermatids with normal signals (Pt-LIS1/Pt-DHC) after *Pt-Lis1* silencing in vivo. (K-N) Number of spermatids with normal signals (Pt-LIS1/Pt-DIC) after *Pt-Lis1* silencing in vivo. "ns" indicates no significant difference, $P > 0.05$, "*" indicates a significant difference, $P < 0.05$, "**" indicates an extremely significant difference, $P < 0.01$; Scale bar = 10 μm.

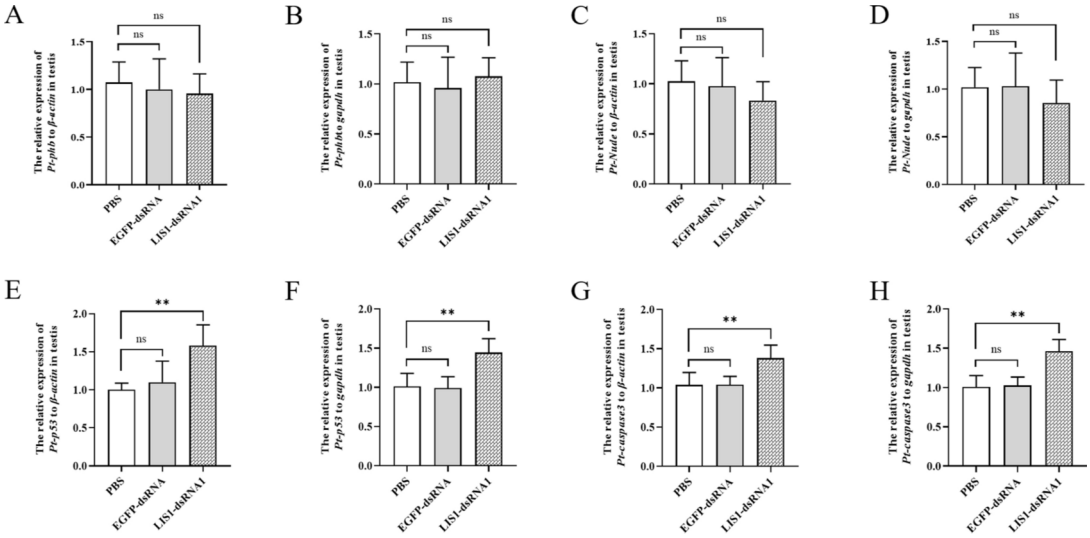

Fig. 11. The relative expression of *Pt-Nude*, *phb*, *p53* and *caspase-3* after *Pt-Lis1* silencing. (**A**, **B**) The expression of *phb* in the testis did not change significantly. (**C**, **D**) The expression of *Pt-Nude* in the testis did not change significantly. (**E**, **F**) The expression of *p53* in the testis was significantly increased. (G, H) The expression of *caspase-3* in the testis was significantly increased. "ns" means no significant difference, $P > 0.05$, "*" means a significant difference, $P < 0.05$, "**" means an extremely significant difference, $P < 0.01$.

Multiple sequence alignment, phylogenetic evolutionary tree analysis and protein structure prediction

The amino acid sequence of Pt-LIS1 was obtained by the Sequence Manipulation Suite (SMS) (http://www.bio-soft.net/sms/); the molecular weight and isoelectric point of Pt-LIS1 were predicted by using the ExPASy-ProtParam tool (https://web.expasy.org/protparam/); the secondary structure and conserved structural domains of Pt-LIS1 were predicted by the SMART (http://smart.embl-heidelberg.de/) software and the CD-Search tool from the NCBI website (https://www.ncbi.nlm.nih.gov/Structure/cdd/wrpsb.cgi). The protein 3D structure of Pt-LIS1 was predicted by the online software I-TASSER (https://zhanggroup.org/I-TASSER/). Sequence alignment and phylogenetic analyses were performed with the software Vector NTI10 (Invitrogen, California, USA) and Mega 5.1 (Informar Technologies, USA), respectively. The amino acid (aa) sequences of LIS1 proteins were downloaded from the National Center of Biotechnology Information (https://www.ncbi.nlm.nih.gov/), and their GenBank accession numbers are listed in Supplementary Table 3.

Expression analysis of *Pt-Lis1* mRNA in different tissues of *P. trituberculatus*

Semiquantitative RT-PCR was conducted to distinguish the *Pt-Lis1* mRNA expression of different tissues of *P. trituberculatus*. We used the reversed cDNA of the testis, muscle, gill, hepatopancreas and vas deferens for

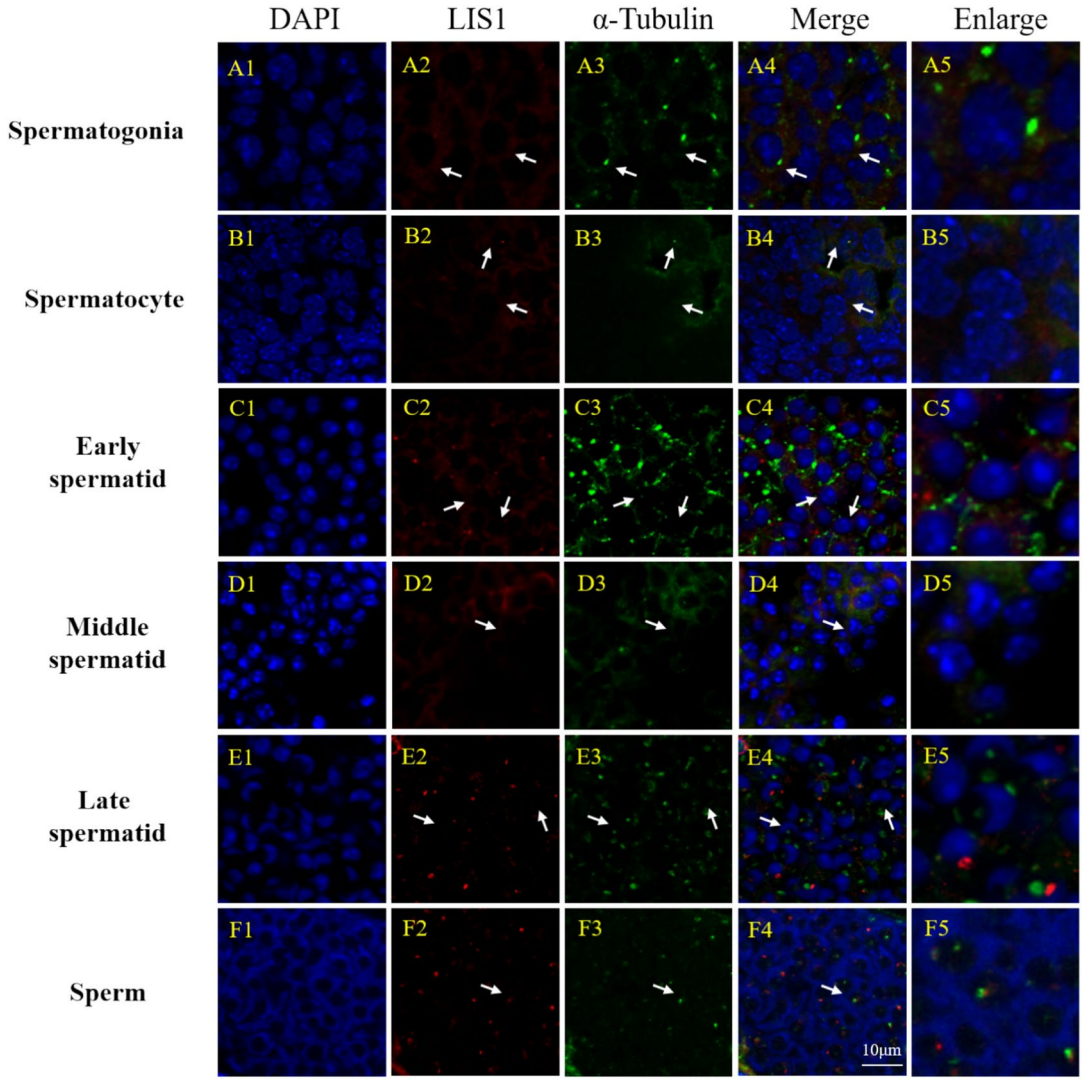

Fig. 12. Colocalization of Pt-LIS1 and α-Tubulin proteins during spermatogenesis was diminished after *Pt-Lis1* silencing in vivo. (A1-A5) Spermatogonia; (B1-B5) Secondary spermatocytes; (C1-C5) Early spermatids; (D1-D5) Middle spermatids; (E1-E5) Late spermatids; (F1-F5) Mature sperm. The blue color indicates the nuclei stained with DAPI; the red color indicates Pt-LIS1; the green color indicates α-Tubulin, and the arrows indicated that the typical signals of Pt-LIS1 and Pt-DIC. N: nuclear; AC: acrosome cap; AT: acrosome tube; MC: membrane complex; FL: fibrous layer; ML: intermediate layer; LS: lamellar structure; RA: radial arm. Scale bar = 10 μm.

semiquantitative RT-PCR. We designed different pairs of primers for *Pt-Lis1* and the control, *β-actin*. PCR programs were set as follows: 94 °C for 5 min; 32 cycles of 94 °C for 30 s, 56 °C for 30 s, and 72 °C for 20 s; 72 °C for 10 min for the final extension. The products were examined by electrophoresis on a 1% agarose gel. The bands were revealed by DNA gel green and analyzed by ImageJ software. One-way ANOVA was performed on the data using Tukey's HSD and Tukey s-b post hoc tests in IBM SPSS Statistics 25.0 software, and graphs were made using GraphPad Prism 8.0.2 software.

Fluorescence in situ hybridization

The frozen testis sections were fixed in 4% paraformaldehyde in PBS at 4 °C for 18 h, washed twice with 1 × PBS, immersed in 0.5 M sucrose-PBS solution (pH = 7.4) overnight at 4 °C, placed in O.C.T. compound, and frozen at −80 °C. The embedded blocks were cut into slices (5 μm) using a sliding microtome and subsequently adhered to RNase-free poly-lysine-coated slides, which were stored at −80 °C until further use. We designed the reverse primer in the non-conserved sequence region of *Pt-Lis1* cDNA, BLASTed it specifically in the genome of *P. trituberculatus*, and then sent it to Jinweizhi Biotechnology Co. to synthesize the 5´-FAM-modified probe. At the same time, the complementary sequences of the reverse primer were used as the negative control (LIS1-C-probe). The frozen sections were dried and permeabilized and then incubated with the probe at room temperature for 2 h. After incubation, the sections were washed with PBS, stained with DAPI, sealed with a

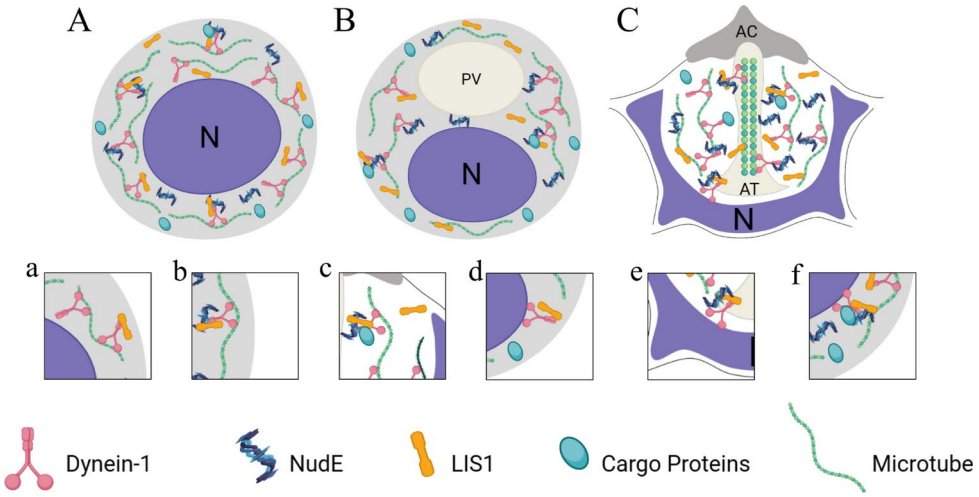

Fig. 13. Expression and potential functional pattern of Pt-LIS1 during spermiogenesis in *P. trituberculatus*. (A, B) Early and middle stages of spermatids. Pt-LIS1 colocalized with Dynein-1 (Pt-DHC and Pt-DIC), NudE (another regulator of Dynein-1) and α-Tubulin, exhibiting a random distribution in the perinuclear cytoplasm. (C) Mature sperm. Pt-LIS1, α-Tubulin and Dynein-1 could be detected in the subacrosomal space, acrosome cap and acrosome tube. Based on the expression of Pt-LIS1 and its colocalization with Dynein-1, α-Tubulin and cargo proteins (mitochondria, Acrosin), it is reasonable to conjecture that, during spermiogenesis, (a). Pt-LIS1 may bind Dynein-1 and (b). the NudE, allowing Dynein-1 to (c). transport cargoes along microtubes to promote nuclear deformation and acrosome formation. Furthermore, (d-f) Pt-LIS1 may position MTs close to the nucleus and promote contraction of the MT network, which may be advantageous for the promotion of nuclear deformation and acrosome formation. N: nuclear; AC: acrosome cap; AT: acrosome tube; MC: membrane complex; FL: fibrous layer; ML: intermediate layer; LS: lamellar structure; RA: radial arm.

drop of anti-fluorescent bursting agent, and finally observed with a Zeiss laser scanning confocal microscope (LSM880, Carl Zeiss, Germany).

Western blot analysis

The specificity of the rat/rabbit anti-Pt-LIS1 antibody was checked by Western blot based on our previous method[9], and only one protein band of approximately 46 kDa was detected, coincident with the predicted molecular weight of Pt-LIS1 (Fig. 3). Therefore, IF could be carried out using the rat/rabbit anti-Pt-LIS1 antibody. In addition, we purchased a rabbit anti-β-actin antibody (Cat. No. AF5003), rabbit anti-α-Tubulin antibody (Cat. No. AF0001), HRP-conjugated goat anti-rat IgG (H + L) (Cat. No. A0192), HRP-conjugated goat anti-rabbit IgG (H + L) (Cat. No. A0208), Cy3-labeled goat anti-rat IgG (H + L) (Cat. No. A0507), Alexa Fluor 555-labeled donkey anti-mouse IgG (H + L) (Cat. No. A0460) and Alexa Fluor 488-labeled goat anti-rabbit IgG (H + L) (Cat. No. A0423) from Beyotime (Shanghai, China). In addition, the rabbit anti-Pt-DHC antibody, rat anti-Pt-DIC antibody, rabbit-anti-PHB antibody and rabbit-anti-acrosin antibody were made in our laboratory, and their specificity has been verified[52] (Supplementary information file).

Immunofluorescence

The experiments were implemented as described in our previous report[9]. The frozen sections were removed from storage at −80 °C and dried for approximately 15 min at room temperature. The dried frozen sections were permeabilized with 0.3% PBST (0.3% Triton X-100 in PBS buffer) for 15 min and then soaked in 5% BSA-PBS (bovine serum albumin in PBS buffer) for 2 h, followed by incubation with primary antibodies (rat/rabbit anti-Pt-LIS1 antibody, rabbit anti-Pt-DHC antibody, rat anti-Pt-DIC antibody, mouse anti-α-Tubulin antibody, rabbit-anti-PHB antibody and rabbit-anti-Acrosin antibody, 1:50 dilution) overnight at 4 °C. Subsequently, the sections were washed with 0.1% PBST three times for 45 min. The washed sections were incubated with secondary antibodies (Cy3-labeled goat anti-rat IgG (H + L), Alexa Fluor 488-labeled goat anti-rabbit IgG (H + L) and Alexa Fluor 555-labeled donkey anti-mouse IgG (H + L), 1:500 dilution) for 2 h at 37 °C. After washing six times with 0.1% PBST for 90 min, the sections were stained with DAPI (Beyotime, Shanghai, China) for 5 min and mounted. Finally, a Zeiss laser scanning confocal microscope (LSM880, Carl Zeiss, Jena, Germany) was used to observe the fluorescence signal. The control groups were incubated with antibody diluent without the primary antibodies.

Hematoxylin and eosin staining

Testes of *P. trituberculatus* were fixed in 4% paraformaldehyde, dehydrated through a graded ethanol series, cleared in xylene, and embedded in paraffin. Sections (5 μm) were stained with hematoxylin for 5 min, differentiated in 1% acid alcohol, blued under running water, and counterstained with eosin for 3 min. After dehydration and clearing, sections were mounted with neutral balsam. Stained sections were observed under

a light microscope (Olympus BX53, Tokyo, Japan) to analyze the histological features and the distribution of spermatogenic cells at different developmental stages.

Effect of *Pt-Lis1* knockdown on the mRNA expression of *Pt-dhc*, *Pt-dic*, *Pt-Nude*, *phb*, *caspase-3* and *p53*

RT-PCR was used to detect the effect of *Pt-Lis1* knockdown on the mRNA expression of *Pt-dhc, Pt-dic, Pt-Nude, phb, caspase-3 and p53*. *β-actin* and *gapdh* were used as the reference genes. The comparative ΔCt method was used to analyze gene expression. The primers are shown in Supplementary Table 4.

Effect of *Pt-Lis1* knockdown on the spatial expression distribution of Pt-LIS1 with Pt-DHC, Pt-DIC and microtubules

IF was used to detect the changes in the colocalization distribution of Pt-LIS1 with Pt-DHC, Pt-DIC, and microtubule (α-Tubulin) in the spermatogenesis of *P. trituberculatus* after *Pt-Lis1* silencing (n = 5).

Statistical analysis

We used GraphPad Prism 8 (GraphPad software, California, USA) for data analysis. All the results are presented as the means ± standard errors of the means. Significance tests using an unpaired t test were performed between the control group and the experimental group. All experiments were repeated three times using different samples. $P < 0.05$ was considered to indicate a significant difference between the control group and experimental group.

Additional information

Data availability

All data generated or analysed during this study are included in this published article (and its Supplementary Information files).

Received: 3 June 2024; Accepted: 16 December 2024
Published online: 24 February 2025

References

1. Oakberg, E. F. A description of spermiogenesis in the mouse and its use in analysis of the cycle of the seminiferous epithelium and germ cell renewal. *Am. J. Anat.* **99**, 391–413 (1956).
2. Vallee, R. B. & Sheetz, M. P. Targeting of motor proteins. *Science.* **271**, 1539–1544 (1996).
3. Fawcett, D. W. The mammalian spermatozoon. *Dev. Biol.* **44**, 394–436 (1975).
4. Breed, W. G. Evolution of the spermatozoon in muroid rodents. *J. Morphol.* **265**, 271–290 (2005).
5. Koch, R. A. & Lambert, C. C. Ultrastructure of sperm, spermiogenesis, and sperm-egg interactions in selected invertebrates and lower vertebrates which use external fertilization. *J. Electron. Micros.c Tech.* **16**, 115–154 (1990).
6. Feng, T., Paterson, B. & Johnston, S. A morphological study of the male reproductive tract, post-testicular acrosome maturation and spermatophore formation in the black tiger prawn (*Penaeus monodon*). *J. Morphol.* **279**, 1290–1300 (2018).
7. Zeng, J., Peng, S., Zhong, S. & Zhang, H. The Spermatozoal Ultrastructure of the Chinese Mitten Crab (*Eriocheir sinensis*). *J. Microsc. Ultrastruct.* **7**, 181–184 (2019).
8. Camargo, T. R. et al. Sperm ultrastructure of shrimps from the family Penaeidae (Crustacea: Dendrobranchiata) in a phylogenetic context. *Arthropod. Struct. Dev.* **46**, 588–600 (2017).
9. Chang, L. et al. Transport of Acrosomal Enzymes by KIFC1 via the Acroframosomal Cytoskeleton during Spermatogenesis in *Macrobrachium rosenbergii* (Crustacea, Decapoda, Malacostracea). *Animals.* **12**, 991 (2022).
10. Medina, A. & Rodriguez, A. Structural changes in sperm from the fiddler crab, Uca tangeri (Crustacea, Brachyura), during the acrosome reaction. *Mol. Reprod. Dev.* **33**, 195–201 (1992).
11. Supp, D. M., Potter, S. S. & Brueckner, M. Molecular motors: the driving force behind mammalian left-right development. *Trends. Cell. Biol.* **10**, 41–45 (2000).
12. Susalka, S. J. & Pfister, K. K. Cytoplasmic dynein subunit heterogeneity: implications for axonal transport. *J. Neurocytol.* **29**, 819–829 (2000).
13. Höök, P. & Vallee, R. B. The dynein family at a glance. *J. Cell. Sci.* **119**, 4369–4371 (2006).
14. Karki, S. & Holzbaur, E. L. Cytoplasmic dynein and dynactin in cell division and intracellular transport. *Curr. Opin. Cell. Biol.* **11**, 45–53 (1999).
15. Wen, Q. et al. Dynein 1 supports spermatid transport and spermiation during spermatogenesis in the rat testis. *Am. J. Physiol. Endocrinol. Metab.* **315**, E924-e948 (2018).
16. Wei, C. G., Mu, D. L., Tang, D. J., Zhu, J. Q. & Hou, C. C. Expression and functional analysis of cytoplasmic dynein during spermatogenesis in *Portunus trituberculatus*. *Cell Tissue Res.* **386**, 191–203 (2021).
17. Xiang, Q. et al. Molecular Cloning of Dynein Heavy Chain and the Effect of Dynein Inhibition on the Testicular Function of *Portunus trituberculatus*. *Animals* **11**, 3582 (2021).
18. Kardon, J. R. & Vale, R. D. Regulators of the cytoplasmic dynein motor. *Nat. Rev. Mol. Cell. Biol.* **10**, 854–865 (2009).
19. McKenney, R. J. LIS1 cracks open dynein. *Nat. Cell. Biol.* **22**, 515–517 (2020).
20. Smith, D. S. et al. Regulation of cytoplasmic dynein behaviour and microtubule organization by mammalian Lis1. *Nat. Cell. Biol.* **2**, 767–775 (2000).
21. Swan, A., Nguyen, T. & Suter, B. Drosophila Lissencephaly-1 functions with Bic-D and dynein in oocyte determination and nuclear positioning. *Nat. Cell. Biol.* **1**, 444–449 (1999).
22. Nayernia, K. et al. Inactivation of a testis-specific Lis1 transcript in mice prevents spermatid differentiation and causes male infertility. *J. Biol. Chem.* **278**, 48377–48385 (2003).
23. Mesngon, M. T. et al. Regulation of cytoplasmic dynein ATPase by Lis1. *J. Neurosci.* **26**, 2132–2139 (2006).
24. Dawe, A. L., Caldwell, K. A., Harris, P. M., Morris, N. R. & Caldwell, G. A. Evolutionarily conserved nuclear migration genes required for early embryonic development in *Caenorhabditis elegans*. *Dev. Genes. Evol.* **211**, 434–441 (2001).
25. Sitaram, P., Anderson, M. A., Jodoin, J. N., Lee, E. & Lee, L. A. Regulation of dynein localization and centrosome positioning by Lis-1 and asunder during Drosophila spermatogenesis. *Development.* **139**, 2945–2954 (2012).

26. Yamada, M. et al. LIS1 and NDEL1 coordinate the plus-end-directed transport of cytoplasmic dynein. *Embo. J.* **27**, 2471–2483 (2008).
27. Moon, H. M. et al. LIS1 controls mitosis and mitotic spindle organization via the LIS1-NDEL1-dynein complex. *Hum. Mol. Genet.* **23**, 449–466 (2014).
28. Williams, S. N., Locke, C. J., Braden, A. L., Caldwell, K. A. & Caldwell, G. A. Epileptic-like convulsions associated with LIS-1 in the cytoskeletal control of neurotransmitter signaling in *Caenorhabditis elegans*. *Hum. Mol. Genet.* **13**, 2043–2059 (2004).
29. Kim, M. H. et al. The structure of the N-terminal domain of the product of the lissencephaly gene Lis1 and its functional implications. *Structure.* **12**, 987–998 (2004).
30. Neer, E. J., Schmidt, C. J., Nambudripad, R. & Smith, T. F. The ancient regulatory-protein family of WD-repeat proteins. *Nature.* **371**, 297–300 (1994).
31. Geiser, J. R. et al. Saccharomyces cerevisiae genes required in the absence of the CIN8-encoded spindle motor act in functionally diverse mitotic pathways. *Mol. Biol. Cell.* **8**, 1035–1050 (1997).
32. Emes, R. D. & Ponting, C. P. A new sequence motif linking lissencephaly, Treacher Collins and oral-facial-digital type 1 syndromes, microtubule dynamics and cell migration. *Hum. Mol. Genet.* **10**, 2813–2820 (2001).
33. Mateja, A., Cierpicki, T., Paduch, M., Derewenda, Z. S. & Otlewski, J. The dimerization mechanism of LIS1 and its implication for proteins containing the LisH motif. *J. Mol. Biol.* **357**, 621–631 (2006).
34. Jiménez, R., Barrionuevo, F. J. & Burgos, M. Natural exceptions to normal gonad development in mammals. *Sex. Dev.* **7**, 147–162 (2013).
35. Dix, C. I. et al. Lissencephaly-1 promotes the recruitment of dynein and dynactin to transported mRNAs. *J. Cell. Biol.* **202**, 479–494 (2013).
36. Lam, C., Vergnolle, M. A., Thorpe, L., Woodman, P. G. & Allan, V. J. Functional interplay between LIS1, NDE1 and NDEL1 in dynein-dependent organelle positioning. *J. Cell. Sci.* **123**, 202–212 (2010).
37. Gepner, J. et al. Cytoplasmic dynein function is essential in *Drosophila melanogaster*. *Genetics.* **142**, 865–878 (1996).
38. Hirokawa, N. Kinesin and dynein superfamily proteins and the mechanism of organelle transport. *Science.* **279**, 519–526 (1998).
39. Palazzo, R. E., Vaisberg, E. A., Weiss, D. G., Kuznetsov, S. A. & Steffen, W. Dynein is required for spindle assembly in cytoplasmic extracts of *Spisula solidissima* oocytes. *J. Cell. Sci.* **112**, 1291–1302 (1999).
40. Howell, B. J. et al. Cytoplasmic dynein/dynactin drives kinetochore protein transport to the spindle poles and has a role in mitotic spindle checkpoint inactivation. *J. Cell. Biol.* **155**, 1159–1172 (2001).
41. Splinter, D., Tanenbaum, M. E., Lindqvist, A., Jaarsma, D., Flotho, A., Yu, K. L., Grigoriev, I., Engelsma, D., Haasdijk, E. D., Keijzer, N., Demmers, J., Fornerod, M., Melchior, F., Hoogenraad, C. C., Medema, R. H. & Akhmanova, A. Bicaudal D2, dynein, and kinesin-1 associate with nuclear pore complexes and regulate centrosome and nuclear positioning during mitotic entry.. Bicaudal D2, dynein, and kinesin-1 associate with nuclear pore complexes and regulate centrosome and nuclear positioning during mitotic entry. *PLoS. Biol.* **8**, e1000350, (2010).
42. Pavin, N. & Tolić-Nørrelykke, I. M. Dynein, microtubule and cargo: a ménage à trois. *Biochem. Soc. Trans.* **41**, 1731–1735 (2013).
43. Goodson, H. V. & Jonasson, E. M. Microtubules and Microtubule-Associated Proteins. *Cold. Spring. Harb. Perspect. Biol.* **10**, a022608 (2018).
44. Fedotov, S., Korabel, N., Waigh, T. A., Han, D. & Allan, V. J. Memory effects and Lévy walk dynamics in intracellular transport of cargoes. *Phys. Rev. E.* **98** (2018).
45. Artal-Sanz, M. & Tavernarakis, N. Prohibitin and mitochondrial biology. *Trends Endocrinol Metab.* **20**, 394–401. https://doi.org/10.1016/j.tem.2009.04.004 (2009).
46. Steglich, G., Neupert, W. & Langer, T. Prohibitins regulate membrane protein degradation by the m-AAA protease in mitochondria. *Mol. Cell. Biol.* **19**, 3435–3442 (1999).
47. Gao, X. et al. Characterisation, expression and possible functions of prohibitin during spermatogenesis in the silver pomfret *Pampus argenteus*. *Reprod. Fertil. Dev.* **32**, 1084–1098 (2020).
48. Xu, Y. R., Fan, Y. S. & Yang, W. X. Mitochondrial prohibitin and its ubiquitination during spermatogenesis of the swimming crab *Charybdis japonica*. *Gene.* **627**, 137–148 (2017).
49. Qiu, X. et al. Characterization of PHB in the gonadal development of the swimming crab *Portunus trituberculatus*. *Comp. Biochem. Physiol. B. Biochem. Mol. Biol.* **240**, 110338 (2020).
50. Baba, T. et al. Activation and maturation mechanisms of boar acrosin zymogen based on the deduced primary structure. *J. Biol. Chem.* **264**, 11920–11927 (1989).
51. Mao, H. T. & Yang, W. X. Modes of acrosin functioning during fertilization. *Gene.* **526**, 75–79 (2013).
52. Xiang, Q. M. et al. The function of the cytoplasmic dynein light chain PTKM23 in the transport of PTSMAD2 during spermatogenesis in *Portunus trituberculatus*. *Biol Reprod.* **111**, 942–958 (2024).
53. Fatima, R. Drosophila Dynein intermediate chain gene, Dic61B, is required for spermatogenesis. *PLoS. One.* **6**, e27822 (2011).
54. Yoshida, T., Ioshii, S. O., Imanaka-Yoshida, K. & Izutsu, K. Association of cytoplasmic dynein with manchette microtubules and spermatid nuclear envelope during spermiogenesis in rats. *J. Cell. Sci.* **107**, 625–633 (1994).
55. Li, M. G., Serr, M., Newman, E. A. & Hays, T. S. The Drosophila tctex-1 light chain is dispensable for essential cytoplasmic dynein functions but is required during spermatid differentiation. *Mol. Biol. Cell.* **15**, 3005–3014 (2004).
56. Ma, D. D., Pan, M. Y., Hou, C. C., Tan, F. Q. & Yang, W. X. KIFC1 and myosin Va: two motors for acrosomal biogenesis and nuclear shaping during spermiogenesis of *Portunus trituberculatus*. *Cell. Tissue. Res.* **369**, 625–640 (2017).
57. Li, J., Lee, W. L. & Cooper, J. A. NudEL targets dynein to microtubule ends through LIS1. *Nat. Cell. Biol.* **7**, 686–690 (2005).
58. Liebl, M. C. & Hofmann, T. G. The Role of p53 Signaling in Colorectal Cancer. *Cancers.* **13** (2021).
59. Aubrey, B. J., Kelly, G. L., Janic, A., Herold, M. J. & Strasser, A. How does p53 induce apoptosis and how does this relate to p53-mediated tumour suppression?. *Cell. Death. Differ.* **25**, 104–113 (2018).
60. Asadi, M. et al. Caspase-3: Structure, function, and biotechnological aspects. *Biotechnol. Appl. Biochem.* **69**, 1633–1645 (2022).

Acknowledgements

The authors would like to thank the schoolmates in the Laboratory of Reproduction and Development of Ningbo University for their help in this project.

Author contributions

C.C.H. and L.C. co-designed the study, performed the experiments, the statistical analysis and wrote the paper. Q.M.X. and Z.T.L. implemented the investigation and the experimental animals breeding. L.C. and Q.M.X. performed the validation of data. C.C.H. and J.Q.Z. supervised the work and commented on the manuscript. Acquisition of financial resources occurred through C.C.H., C.K.M. and C.L.W. All authors read and approved the final version of manuscript.

Funding

This research was supported by the NSFC-Ningbo Joint Fund for Regional Innovation Development (Project ID:

U23A20248), the Key Project of the Ningbo Natural Science Foundation (Project ID: 2022J071), the National Natural Science Foundation of China (Project ID: 31602140), the National Natural Science Foundation of China (Project ID: 42076087), the Earmarked Fund for CARS-48 (Project ID: CARS-48), the K.C.Wong Magna Fund at Ningbo University, and the Collaborative Innovation Center for Zhejiang Marine High-efficiency and Healthy Aquaculture.

Competing interests

The authors declare that there is no conflict of interest that could be perceived as prejudicing the impartiality of the research reported.

Additional information

Supplementary Information The online version contains supplementary material available at https://doi.org/10.1038/s41598-024-83566-2.

Correspondence and requests for materials should be addressed to C.-C.H.

Reprints and permissions information is available at www.nature.com/reprints.

Publisher's note Springer Nature remains neutral with regard to jurisdictional claims in published maps and institutional affiliations.